Improved rate capability of $LiCoO_2$ cathode material via particle size-control for Li-ion Batteries

Greem Kong

Department of Energy Engineering

(Battery Science and Technology)

Graduate School of UNIST

2016

Improved rate capability of $LiCoO_2$ cathode material via particle size-control for Li-ion Batteries

Greem Kong

Department of Energy Engineering
(Battery Science and Technology)

Graduate School of UNIST

Improved rate capability of $LiCoO_2$ cathode material via particle size-control for Li-ion Batteries

A thesis/dissertation
submitted to the Graduate School of UNIST
in partial fulfillment of the
requirements for the degree of
Master of Science

Greem Kong

6. 28. 2016
Approved by

조 재필

Advisor
Jaephil Cho

Improved rate capability of $LiCoO_2$ cathode material via particle size-control for Li-ion Batteries

Greem Kong

This certifies that the thesis/dissertation of Greem Kong is approved.

6. 28. 2016

Signature

조 재필

Advisor: Jaephil Cho

Signature

정경민

Kyeong-Min Jeong

Signature

Nam-Soon Choi

Contents

Abstract

For those several decades, alternative energy production and energy storage system has been actively studied due to dramatic growing of worldwide energy demands and strengthened enviromnetal regulations. Lithium-ion batteries (LIBs) have been spotlighted as a next generation energy storage system. Because lithium is the most electropositive and lightest metal, thus it has a higher volumetric and gravimetric energy density than others regardless of cell types.

Layered metal oxides have been used for Li-ion battery cathodes as most popular source since the first commercial battery launched by Sony in 1991. $LiCoO_2$ is the most popular cathode material having layered structure. It is practically and widely used in the secondary battery fields for portable devices, due to its advantages. It is easy to manufacture $LiCoO_2$ compared to other cathode materials, leading to facilitate mass production. General manufacturing conducted by conventional solid-state calcination using lithium source and cobalt oxide with stoichiometric calculation.

To enhance the rate capability of electrode material, there are several methods such as coating, doping and down-sizing representatively. Herein, we tried to develop the $LiCoO_2$ material showing stable charge rate performance at high rate. The single crystal with big size morphology usually has good electric conductivity and relatively lower ionic conductivity. In contrast, polycrystalline shows vice versa. Therefore, in this experiment we suggested the spherical secondary particle to secure porosity and better tap density compared to existing down-sized particles at the same time.

List of figures

List of tables

I. Introduction

For those several decades, alternative energy production and energy storage system has been actively studied due to dramatic growing of worldwide energy demands and strengthened enviromnetal regulations. As shown in Figure 1, the slope of World annaual consumption to year is getting rapid as years go by. The needs for energy are still increasing with developing industry and technology, despite a price advance of fossil fuel and decreasing of its reserves. Accordingly, it is necessary to replace the fossil fuels with renewable energy such as solar, wind, hydroelectric, geothermal heat, wave energy and etc. However, it should be stored in energy storage devices such as batteries to achieve efficient and proper use.

In particular, coming into wide use of portable electronic devices leads to high demands for small and light energy storage system, which is called battery. Moreover, development of large-scale batteries were also drawn increasing attentions in the various area such as electric vehicles(EVs), hybrid electric vehicles(HEVs),[1] energy storage systems(ESSs) or smart grid systems. Therefore, it is essential to find materials which has high power and high energy density applying to batteries.

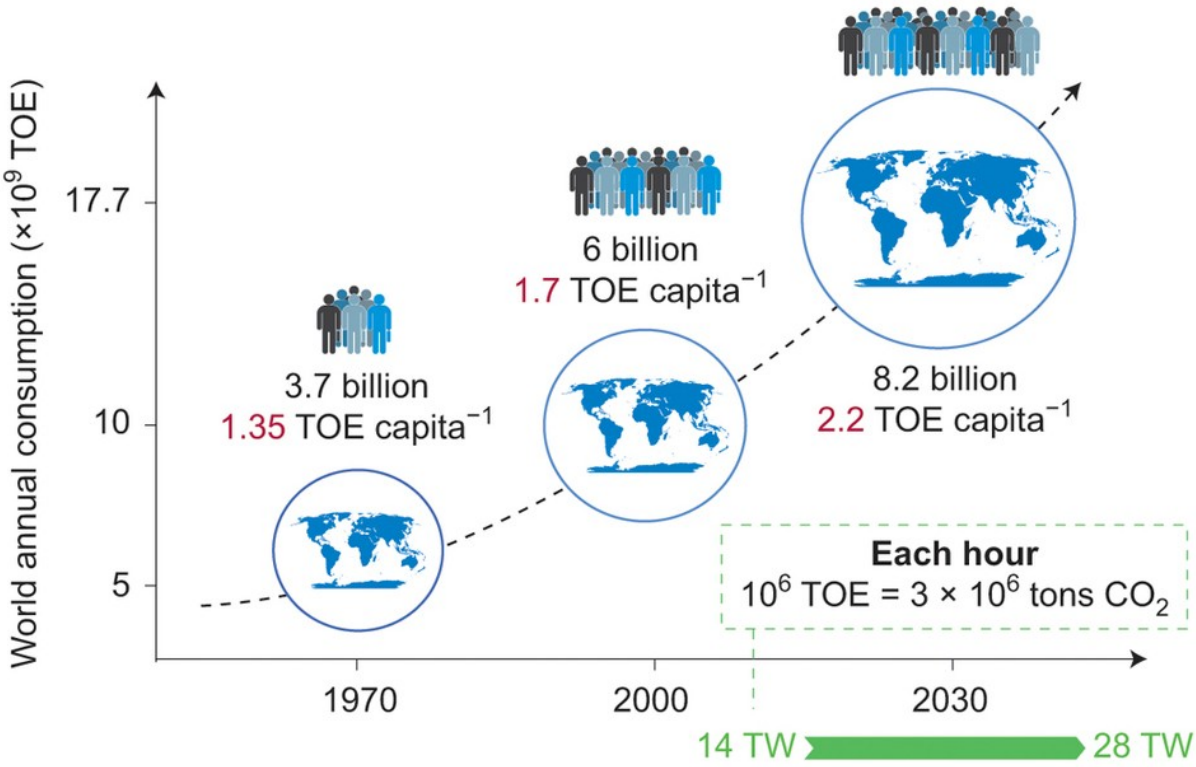

Figure 1. Past, present and forecast of the world's energy needs up to 2050.[2]

1.1 Lithium-ion batteries

1.1.1 Advatages of Lithium-ion batteries

Chemical batteries can be categorized by primary batteries, secondary batteries. Chemical batteries are devices converting chemical energy into electric energy through electrochemical reaction. Primary batteries are disposable type such as alkaline battery, mercury cell. On the contrast, secondary batteries are rechargeable system which can repeat charge and discharge process. Energy storage system needs secondary type.

Lithium-ion batteries (LIBs) have been spotlighted as a next generation energy storage system. Because lithium is the most electropositive and lightest metal, thus it has a higher volumetric and gravimetric energy density than others regardless of cell types as shown in figure 2. Also, it is organic electrolytes based system, which guarantee higher working voltage compared to that of water electrolyte. Therefore, LIBs offer a high power density. Furthermore, it has a stable cyclability, no memory effect and a reasonable price.

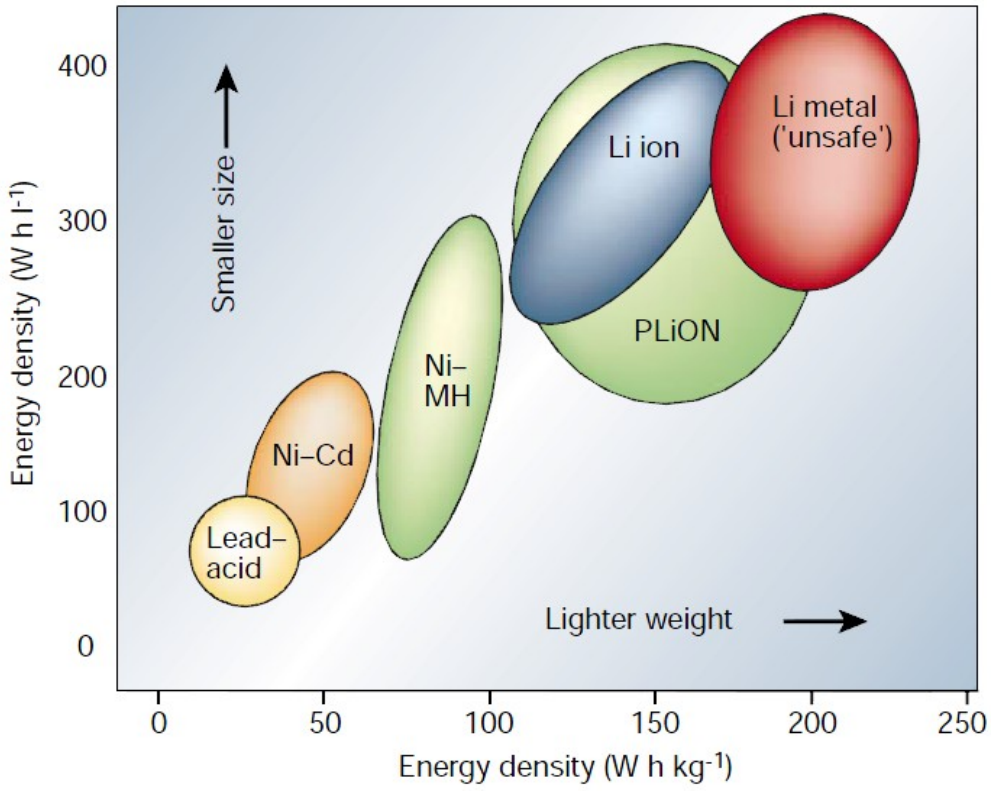

Figure 2. Comparison of the different battery technologies in terms of volumetric and gravimetric energy density.[3]

SONY launched the first commercialization of Lithium-ion battery in 1991, consisted of $LiCoO_2$ as the cathode material and graphite as the anode material. It replaced the lithium metal used as an anode material before, performed as a much safer secondary battery compared to prior type.

Battery Type	Voltage Range (V)	Energy Density (Wh/L)	Specific Energy (Wh/kg)	Specific Power (W/kg)	Cycleability
Lead Acid[52]	2.1 - 1.8	60 - 75	30 - 40	60 - 110	100 - 500
Nickel-Cadmium[53,54]	1.3 - 0.8	130 - 150	40 - 60	40 - 100	2000
Nickel-Metal Hydride[55,56]	1.3 - 0.9	250 - 330	70 - 100	70 - 200	1000
Lithium Ion - $Li(TM)O_2$ - C TM = Ni, Co, Mn[52,38]	4.2 - 2.5	200 - 250	120 - 160	200 - 300	300 - 1000
Lithium Ion - $LiFePO_4$ - C[57]	3.5 - 2.5	120 - 150	80 - 90	200 - 300	1500 - 2000
Lithium Metal-Polymer[58,59]	4.0 - 2.4	100 - 110	100 - 110	130 - 170	600
Sodium-Sulfur[60]	2.1 - 1.8	70 - 150	60 - 120	15 - 70	4000
Sodium-Metal Chloride[61]	2.6	20 - 140	50 - 100	30 - 150	3000
Vanadium Redox Flow[62]	1.6 - 1.1	10 - 20	10 - 20	1 - 4	5000

Table 1. Energy and power Characteristics for batteries being considered for grid storage applications. The range of values reflects variations associated with battery design and performance.[4]

1.1.2 Principle of Lithium-ion batteries

Basically, lithium-ion batteries are composed of four components, cathode, anode, electrolyte, and separator.

Cathode electrode: $LiCoO_2 \rightarrow Li_{1-x}CoO_2 + xLi^+ + xe^-$

Anode electrode: $C_6 + xLi^+ + xe^- \rightarrow Li_xC_6$

Overall charge reaction: $LiCoO_2 + C_6 \rightarrow Li_{1-x}CoO_2 + Li_xC_6$

During discharge, lithium ions diffuse from a lithiated graphite ($LixC_6$) structure (the anode) into delithiated $Li_{1-x}CoO_2$ structure (the cathode) with concomitant oxidation and reduction of the two electrodes, respectively. The reverse process occurs during charge. [5]

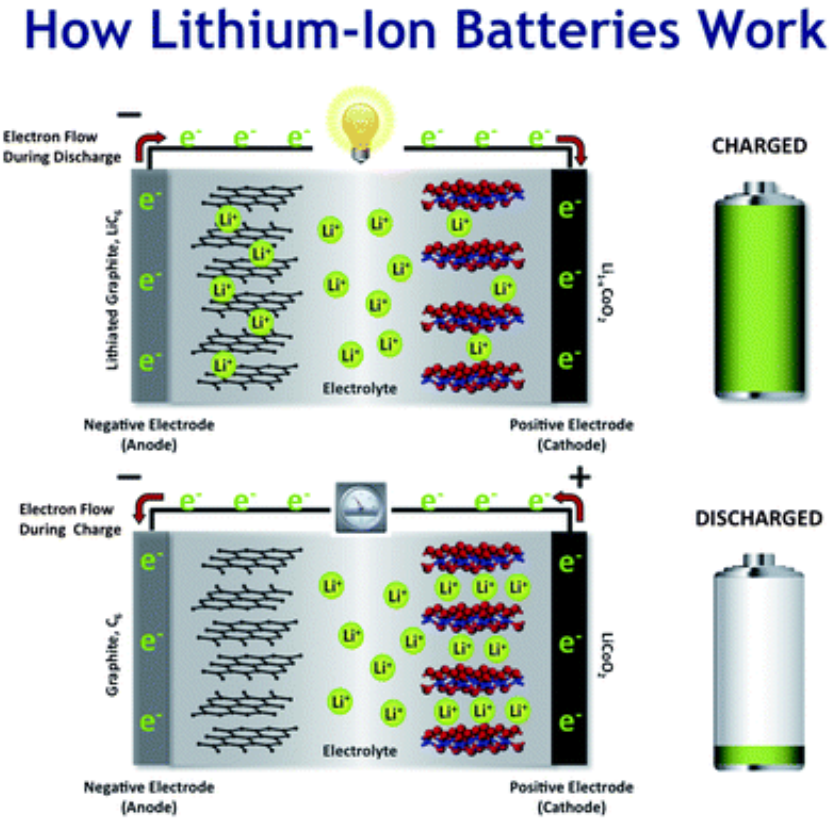

Figure 3. A schematic illustration of the working principles of a $LixC_6$/ $Li_{1-x}CoO_2$ lithium-ion cell. [5]

1.2 Layered $LiCoO_2$ cathode materials for lithium-ion batteries

The Cathode materials for lithium ion batteries are transition metal oxide containing lithium. When charging and discharging, lithium ions should be able to diffuse freely to carry out deintercalation/intercalation through the crystal structure. The transition metal ions are oxidized at the charge process and reduced at the discharge process. The operating voltages are dependent on its structure and transition metal ions. Each materials have own advantages and disadvantages respectively. (Table 2)

Many cathode materials have been extensively developed such as layered ($LiMO_2$, M=Co, Al, Mn and Ni etc.), spinel ($LiMn_2O_4$) and olivine ($LiMPO_4$, M=Fe, Mn and Co etc.) cathode materials since lithium ion batteries were launched in commercial matkets.[6]

	$LiCoO_2$	$LiNi_{0.8}Co_{0.15}Al_{0.05}O_2$	$LiFePO_4$	$LiNi_{0.5}Mn_{1.5}O_4$	$LiMn_2O_4$
Structure	**Layered**	**Layered**	**Olivine**	**Spinel**	**Spinel**
Theoretical Capacity(mAh/g)	**274**	**279**	**170**	**147**	**148**
Available Capacity(mAh/g)	**160**	**185**	**150**	**120**	**110**
Operating Voltage(V) (vs. lithium)	**3.9**	**3.6**	**3.4**	**4.7**	**4.0**
Electrode density (g/cc)	**3.7**	**3.3**	**2.6**	**3.2**	**3.2**
Advantage	**High conductivity Easy synthesis**	**High Capacity**	**Good thermal stability**	**High power**	**Good thermal stability Low price High power**
Disadvantage	**High cost Thermal instability**	**Thermal instability**	**Low conductivity**	**Electrolyte Oxidation**	**Mn dissolution**

Table 2. Comparison of cathode materials for lithium ion batteries.

1.2.1 Layered structure of $LiCoO_2$

Layered metal oxides have been used for Li-ion battery cathodes as most popular source since the first commercial battery launched by Sony in 1991. These materials are made up of slabs of edge sharing MO_6 octahedra (where M is Ni, Co and/ or Mn) separated by layers of Li cations.[7]

The lithium ions are occupied into octahedral sites and transition metal ion are also located into octahedral sites. The ideal $LiMO_2$ crystal belongs to α-$NaFeO_2$ structure family and $R\bar{3}m$ space group with cubic closed packed array of ABCABC type stacking like O-Li-O-TM-O-Li-O along the [111] face. The lithium ions in layered structure materials show 2-dimensional diffusion along the slabs.

The elemental composition of cathode materials has changed in diverse since Sony first used $LiCoO_2$ as an intercalation cathode. Recently doped with Ni and Mn with the formula of $Li[Ni_xMn_yCo_z]O_2$ ($x + y + z = 1$.) widely used and reaserached. [7] The transition metal ratios can be changned to control properties such as capacity, cost, cyclability and operating potential.

Goodenough recognized that $LiCoO_2$ had a structure similar to that of the dichalcogenides (layered structure) and showed that the lithium could be deintercalated electrochemically, thus applied it as a cathode material for lithium-ion batteries.

LiCoO2 belonged to the R3m space group with lattice parameter of a = 2.82 A, c = 14.1/~ in hexagonal.[8]

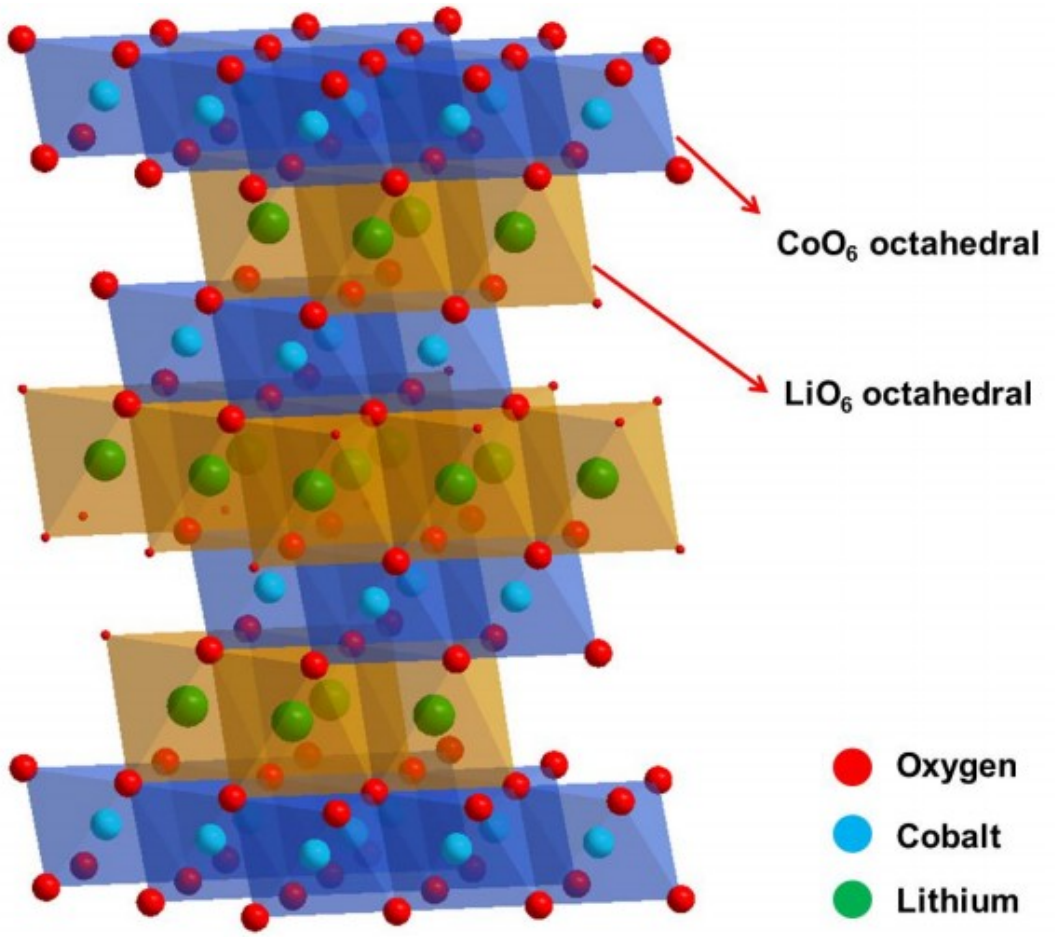

Figure 4. Layered structure of $LiCoO_2$ cathode material.

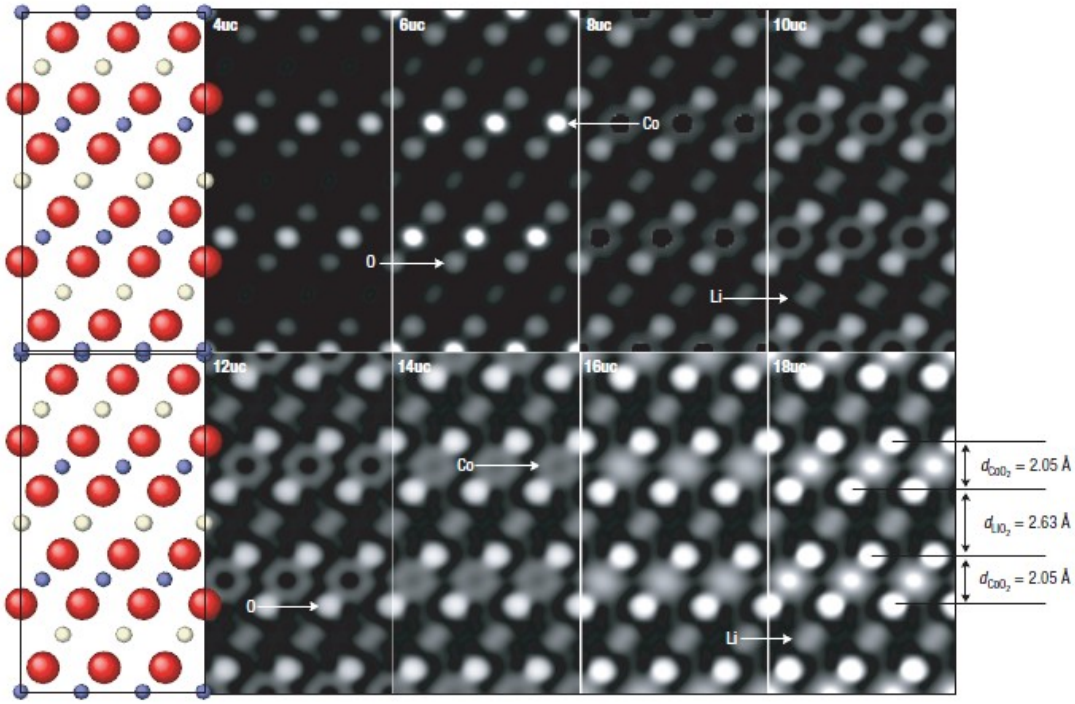

Figure 5. Atomic-resolution images of $LiCoO_2$ in the [110] zone axis show phase peaks at the atom positions. [9]

1.2.2 Advantages/Disadvantages of $LiCoO_2$

$LiCoO_2$ is the most popular cathode material having layered structure. It is practically and widely used in the secondary battery fields for portable devices, due to its advantages.

The attempt to practically apply layered oxides containing lithium ion as cathode materials has begun from the discovery by J.B. Goodenough in 1980 that $LiCoO_2$ shows an electrical potential of 4V and that the reversible insertion and desorption of lithium ion are possible.[10]

First of all, it is easy to manufacture $LiCoO_2$ compared to other cathode materials, leading to facilitate mass production. There are lots of synthetic method such as sol-gel[11], co-precipitation[12], hydrothermal synthesis[13], and ion-exchange[14], etc, so on. Among those lots of method, general manufacturing conducted by conventional solid-state calcination using lithium source (e.g. lithium carbonate) and cobalt oxide with stoichiometric calculation. It is very simple way to process including mixing and calcination.

$LiCoO_2$ can be categorized depending on the calcination temperature, as two type: LT-LCO and HT-LCO. At 400℃, LT-LCO is formed as a spinel $Li_2Co_2O_4$ structure, on the other hand, over 800℃, HT-LCO is synthesized as a layered $LiCoO_2$.[15] But in case of LT-LCO has inner defect of crystal and low crystallinity, accordingly it shows low electrochemical performance.[16] Therefore, usually in commercial market, HT-layered $LiCoO_2$ is chosen.

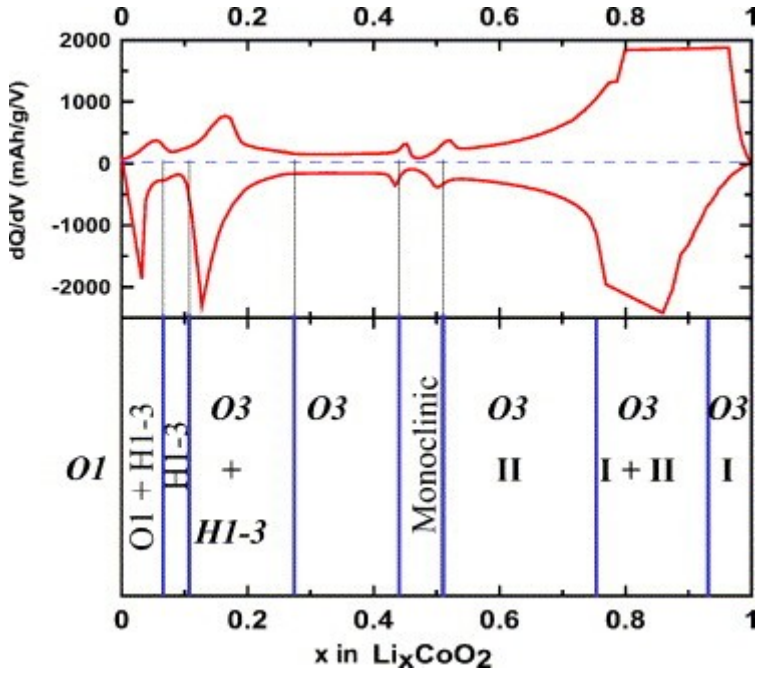

Figure 6. Differential capacity and phase diagram of Li_xCoO_2. [17]

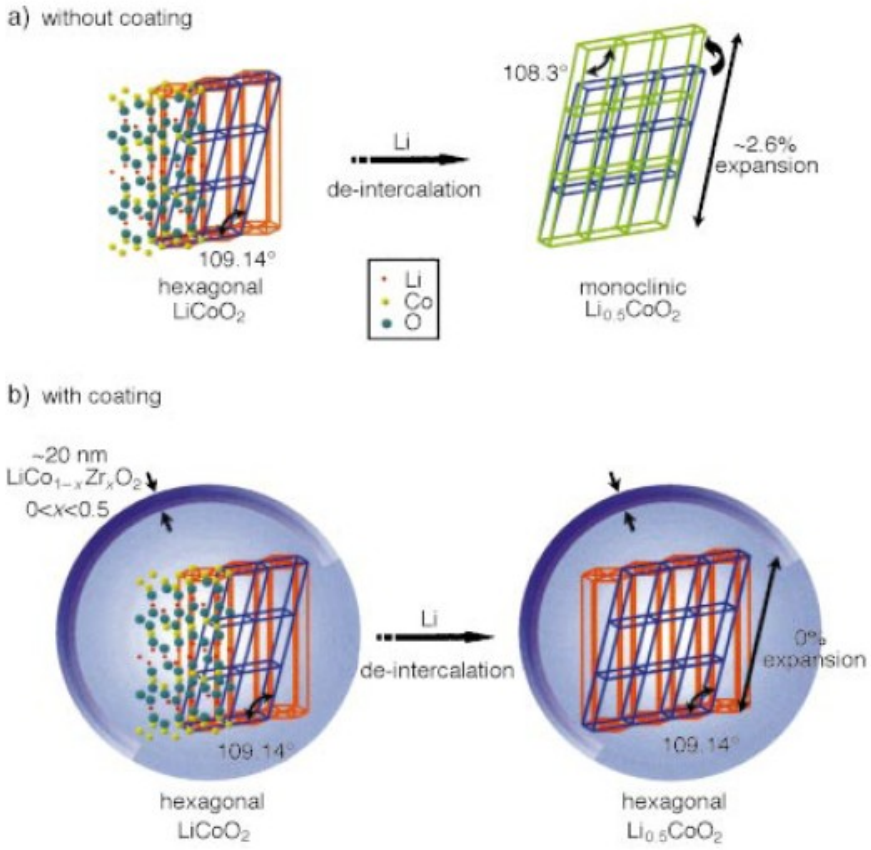

Figure 7. a) The formation of monoclinic phase with non-uniform lattice constant expansion in bare LiCoO2 during charging(Li de-intercalation), and b) the suppression of phase transition from hexagonal to monoclinic phase by a fracture-toughened thin-film metal-oxide coating.[18]

Moreover, it has outstanding electrochemical properties and high electrode density. It provides high voltages of over 4V against a lithium metal anode.[19] It has low possibility to occur irreversible phase transition during charging and discharging as low spin Co^{3+} and Co^{4+} are structurally stable at octahedral sites.[20] But if x>0.5, $Li_{1-x}CoO_2$ undergoes irreversible phase transition from hexagonal to monoclinic (O3 to P3) and it cannot be recovered.(Fig. 6) [21].Thus, despite 274mAhg^{-1} of the theoretical specific capacity of $LiCoO_2$, it shows 137mAhg^{-1} to 150mAhg^{-1} practical specific capacity which is only half of the original.

During the cycling, CoO_2 layer is reconstructed as it is slept, not breaking Co-O bonding, because P3 structure has AABBCC and ABABAB oxygen array.[22] This dimensional change causes a shearing stress between particles finally leads to fractures in lots of oxide.[23] Finally it occurs c-axis expansion (~2.6%, fig 7.a). [18] To overcome this problem, from Cho et al. research group, the surface coating method[24] was proposed using various metal oxide such as ZrO_2, Al_2O_3,[25] TiO_2 and B_2O_3 with nano-sized thickness (Fig 7.b).

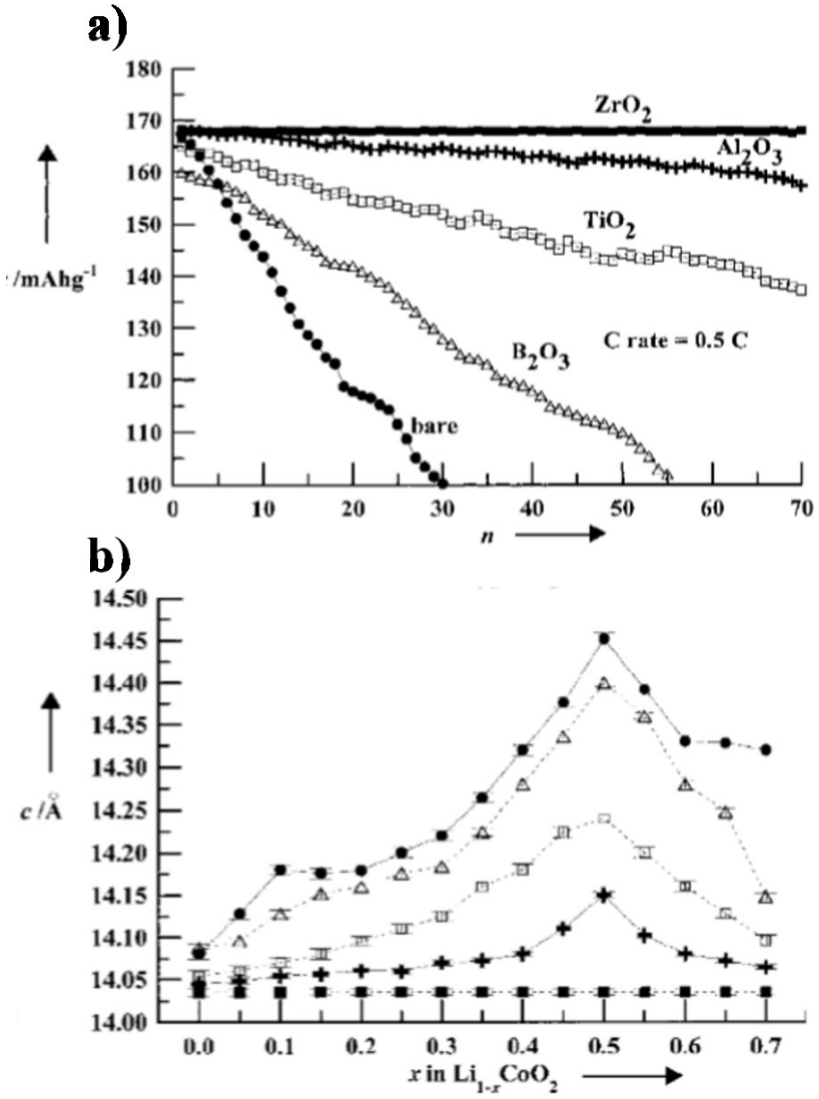

Figure 8. The cycling performance of various coating materials coated $LiCoO_2$ and bare $LiCoO_2$. [18]

Among them, ZrO_2 was show perfectly improved cycle retention closed to zero-strain during intercalation and de-intercalation during 70 cycles (Fig.8). It is related to toughness of metal oxides. Coating layers suppresses dissolution of transition metal and strengthen stability at high voltage. The surface coating method also has influenced on the thermal stability.[26]

1.2.3 Kinetics of Li^+ ion

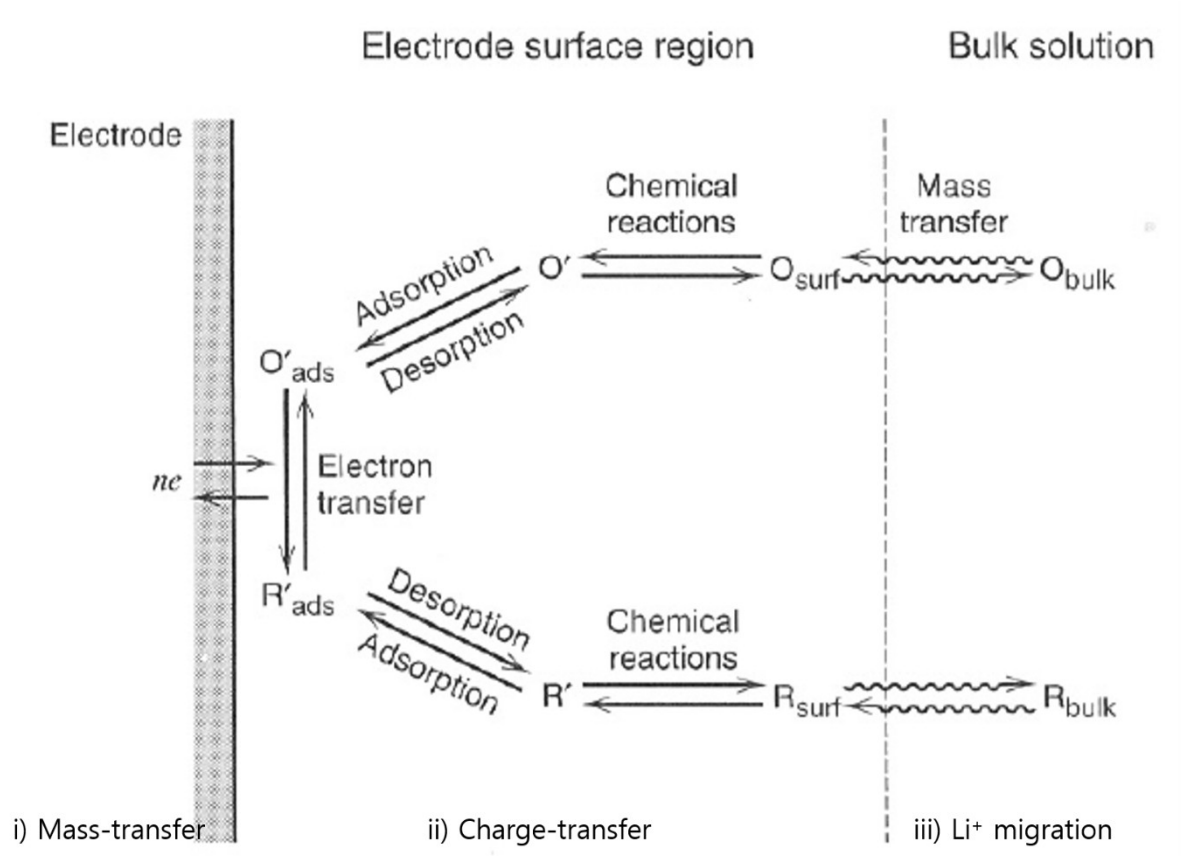

Figure 8. Steps for electrochemical reaction.[27]

We can divide the electrochemical reaction of Li-ion batteries involving three reaction steps. At first, a mass transfer reaction for the solid-state diffusion of Li^+ ions is take place in the structure of the electrode materials. Secondly, a charge-transfer reaction occurs at the interface between the electrode and electrolyte. Finally, the Li^+ migration reaction plays in the electrolyte.[28] The rate capability of the Li-ion batteries is enormously influenced by mass-transfer and charge-transfer reaction.

Using the electrochemical impedance spectroscopy (EIS) analysis method, we can figure out the each resistance factors from Li^+ migration, surface resistance, charge transfer resistance[29] and mass transfer involving Li^+ diffusion[30] element as displayed in figure 9. Electrochemical

impedance spectroscopy (EIS) technique has been used to study the electrode materials because it can reveal the relationship between the crystal lattice with the electrochemical properties.[31]

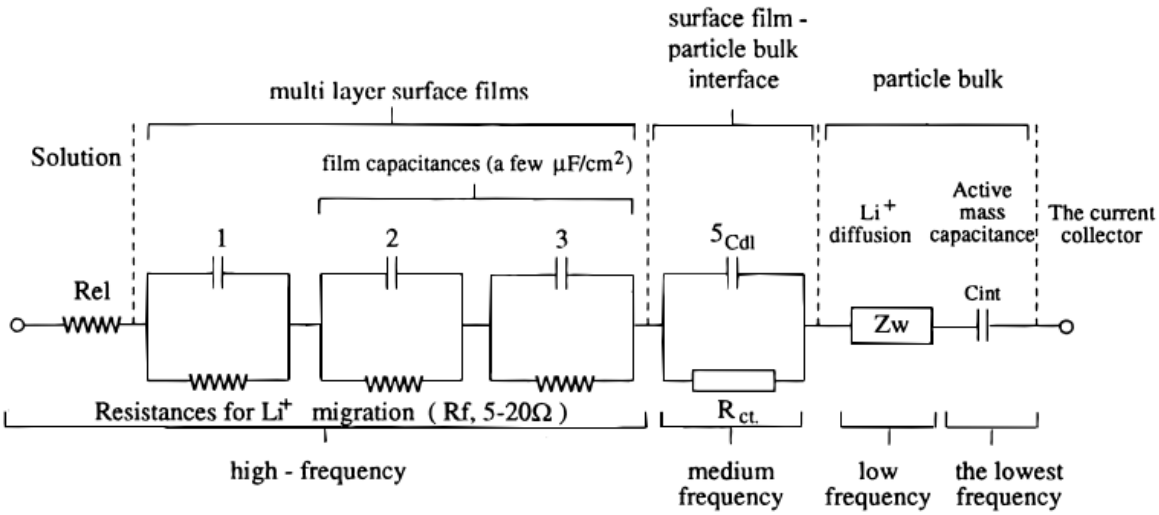

Figure 9. Equivalent circuit analog based on a combination of generalized impedance model. The various time constants to which the model refers are also presented.[30]

1.2.4 Strategies to improve the rate performance at high rate

To enhance the rate capability of electrode material, there are several methods such as coating[32], doping[33] and down-sizing[34] representatively. First of all, there are several coating methods according to coating materials, for instance, the carbon coating to improve electrical conductivity.[35] Carbon sources have higher electric conductivity in usual, it leads to well-maintained electrical connectivity. Scott et al. have conducted the ultrathin Al_2O_3 coating via ALD method as 2Å thickness on the fabricated $LiCoO_2$ of down-sized to 400nm level. As shown in figure 10, the capacity of Nano, 2 ALD $LiCoO_2$ sample is higher than others in overall range of C-rate. The ultrathin thickness allows for a high rate of Li-ion diffusion from inside of particle as well as barely reduce the overall capacity. Furthermore, particle size range is below 1 ㎛, around 400nm in average shortened the Li+ ion insertion distances thus enhancing the power density.

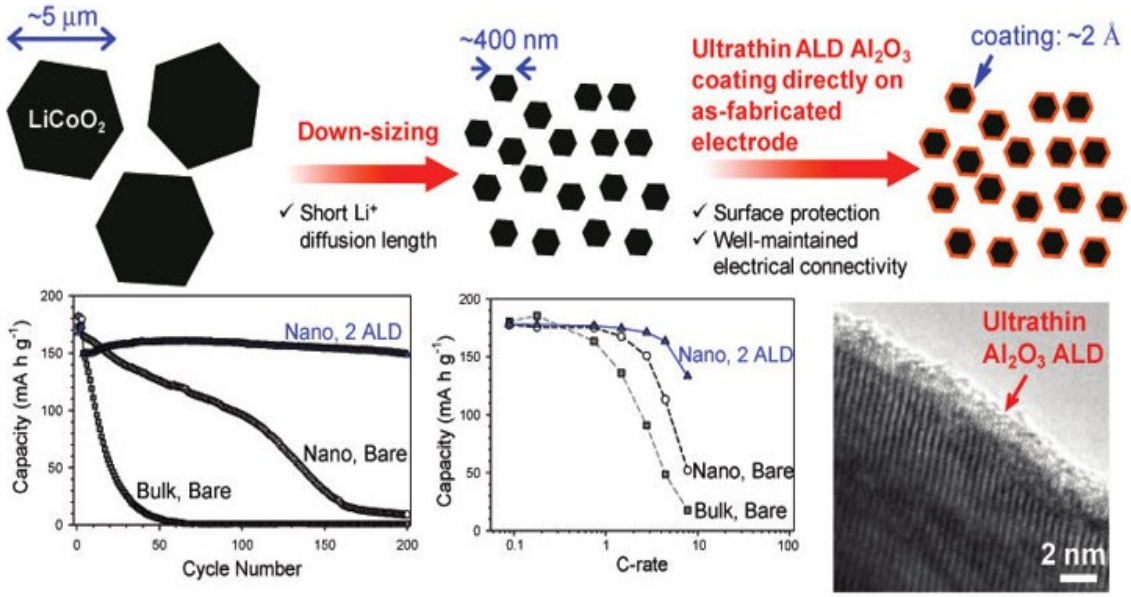

Figure 10. Schematic concepts of ultrathin coating on nano-$LiCoO_2$ for Li-ion vehicular applications. Below three figures display Cycle life, rate property, coating layer confirmed via TEM in order, respectively.[36]

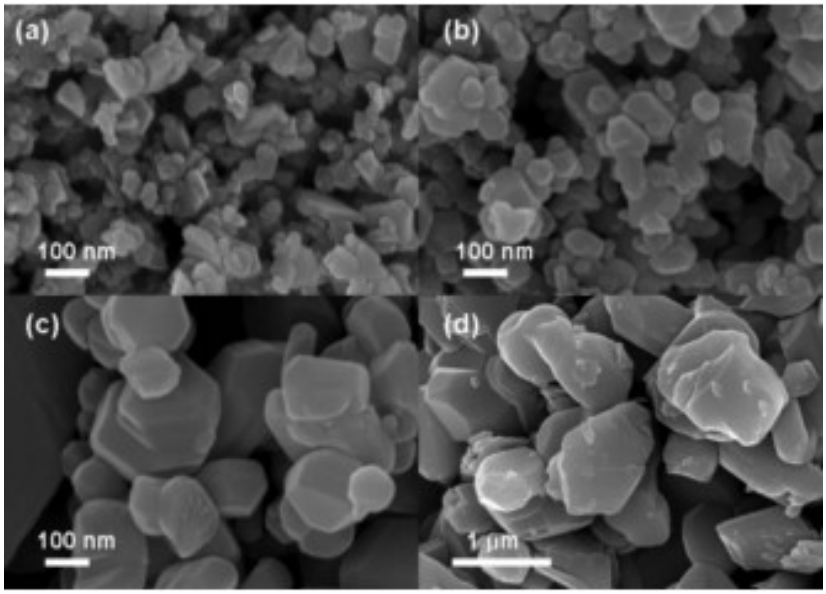

Figure 11. SEM images of the nano-sized $LiCoO_2$ particles obtained at various temperatures via hydrothermal reaction. (a) 200℃, (b) 500℃, (c) 700℃, and (d) 900℃ for 5h.[34c]

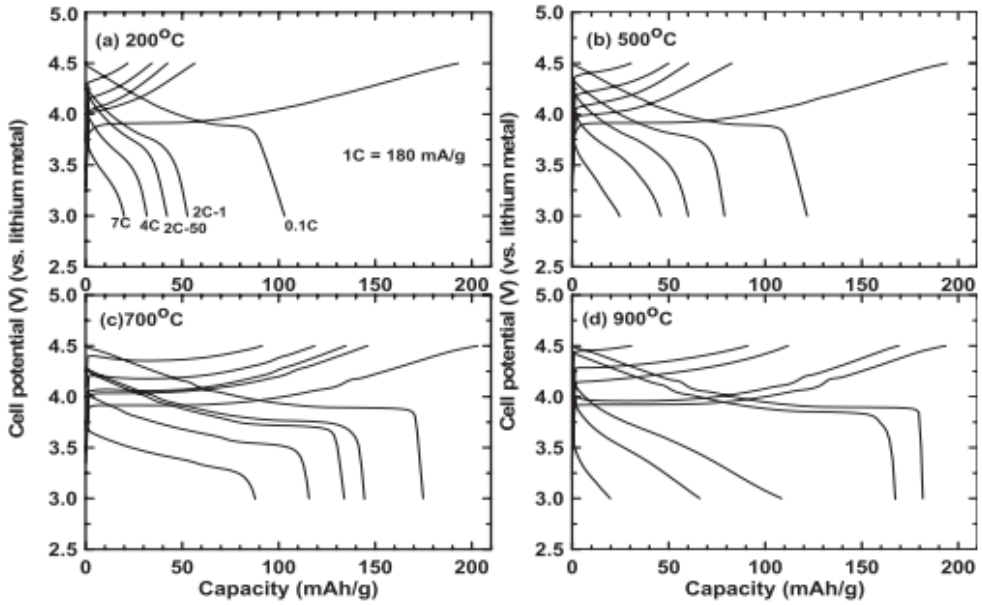

Figure 12. The first cycle voltage profiles of the nano-sized $LiCoO_2$ at 0.2, 2, 4, and 7C rates. [34c]

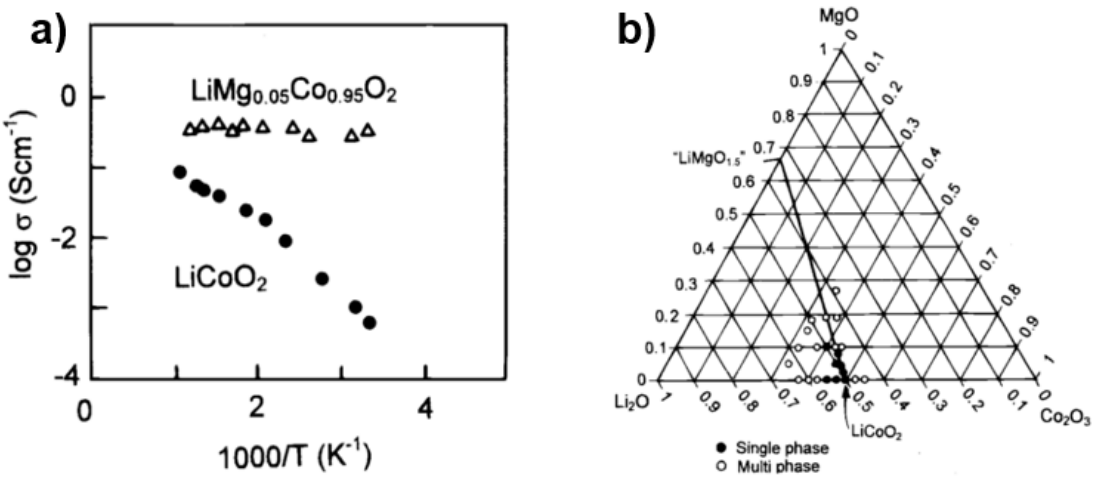

Figure 13. a) Comparision of log scale plot electric conductivity of $LiCoO_2$ and Mg doped $LiMg_{0.05}Co_{0.95}O_2$. b) Phase diagram of the Li_2O-Co_2O_3-MgO sysem. [37]

Secondly, various nano-sized cathode materials have been studied by synthesizing 0D, 1D, 2D, and 3D materials through diverse methods.[38] These nano-sized particles can effectively reduce the diffusion length of lithium ions and increase the active site between electrolyte and cathode materials, which can improve the rate capability at the high current density as shown in figure 11 and 12.[39]

Finally, doping method is also good way to enhance the electronic conductivity as well as structural stability in terms of cycling performance. LiCoO2 the active cathode material in commercial rechargeable lithium batteries[40], is shown to be a p-type semiconductor, associated with the presence of a small concentration of Co4+ ions. Its conductivity can be increased by over two orders of magnitude by partial substitution.[41] It occurs but good reversibility is retained.[33a, 37]

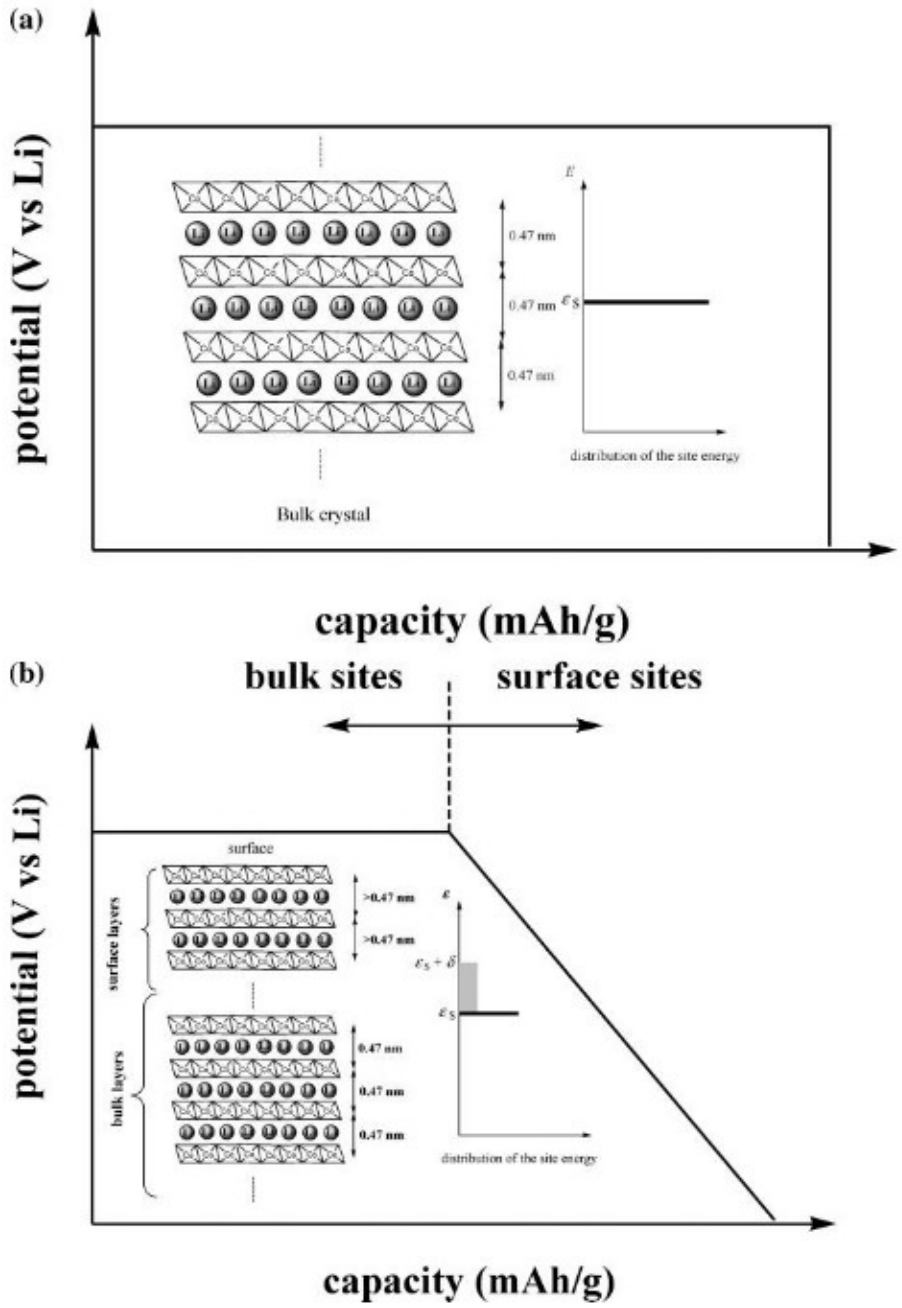

Figure 14. Expected theoretical discharge curve for bulk $LiCoO_2$ and nanocrystalline $LiCoO_2$. (a) Expected discharge curve for bulk $LiCoO_2$, (b) for nanaocrystalline $LiCoO_2$. Disordered structure and the dispersed distribution of the site energy.[34b]

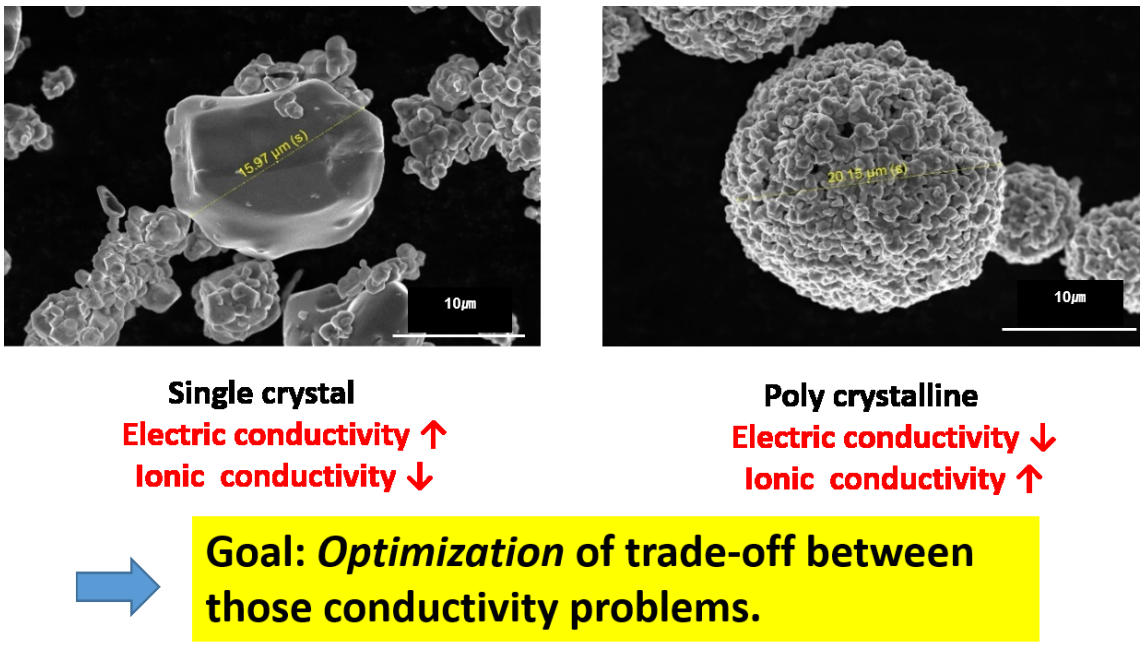

Figure 15. The purpose of experiment to optimize trade-off between electric and ionic conductivity.

Herein, we tried to develop the $LiCoO_2$ material showing stable charge rate performance at high rate. As exhibited in figure 15, the single crystal with big size morphology usually have good electric conductivity and relatively lower ionic conductivity. In contrast, polycrystalline shows vice versa. Therefore, in this experiment we suggested the spherical secondary particle to secure porosity and better tap density compared to existing down-sized particles at the same time. The advantages of this study are like as follows. 1) Higher tap or pellet density compared to existing down-sized nanoscale particles. 2) Improved contact via forming of spherical morphology. 3) Only focused on “size=effect”, no coating.

II. Experimetal Method

2.1 Experimental method

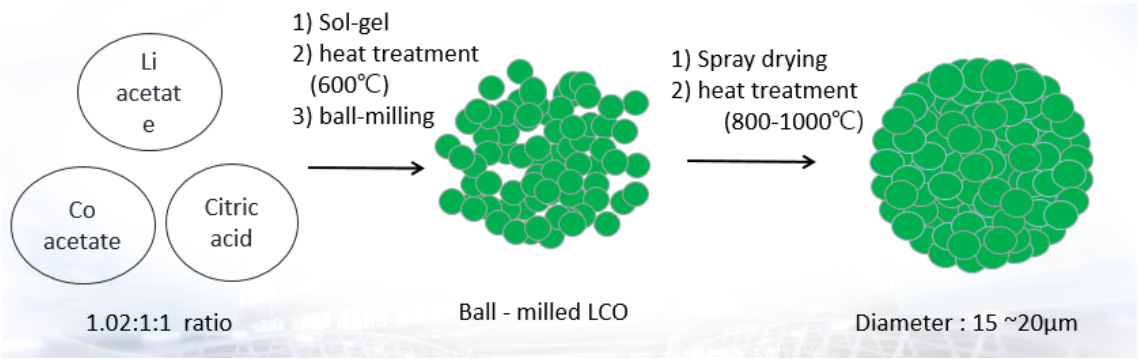

Figure 16. Schematic sequence of synthesized to spherical shape secondary particle of $LiCoO_2$ via sol-gel method and spray-drying.

Bare $LiCoO_2$ was synthesized via sol-gel method using acetate precursors and citric acid.[42] The mole ratio of the each elements is Li: Co: Citric = 1.02: 1: 1. Stoichiometric amounts of lithium acetate dihydrate, cobalt acetate tetrahydrate and citric acid were dissolved into distilled water and heated at 180℃ with strring around 200rpm until dried out. After sol-gel process, to remove remained acetate ingredients and form $LiCoO_2$, it was annealed at 400℃ during 2h and 600℃ during 10h under air atmosphere. In order to spread out primary particles of $LiCoO_2$, synthesized powder underwent ball-milling process during overnight.

Spray drying method was carried out to prepare the sphere-like shape secondary particle composed by primary particle as shown in figure 16, the inlet temperature was 200℃ and pumping rate was 4.5ml/min. Obtained powder were calcinated one more at 900℃ for 10h so that clear layered structure $LiCoO_2$ phase was realized and impurities were removed.

2.2 Electrochemical measurement

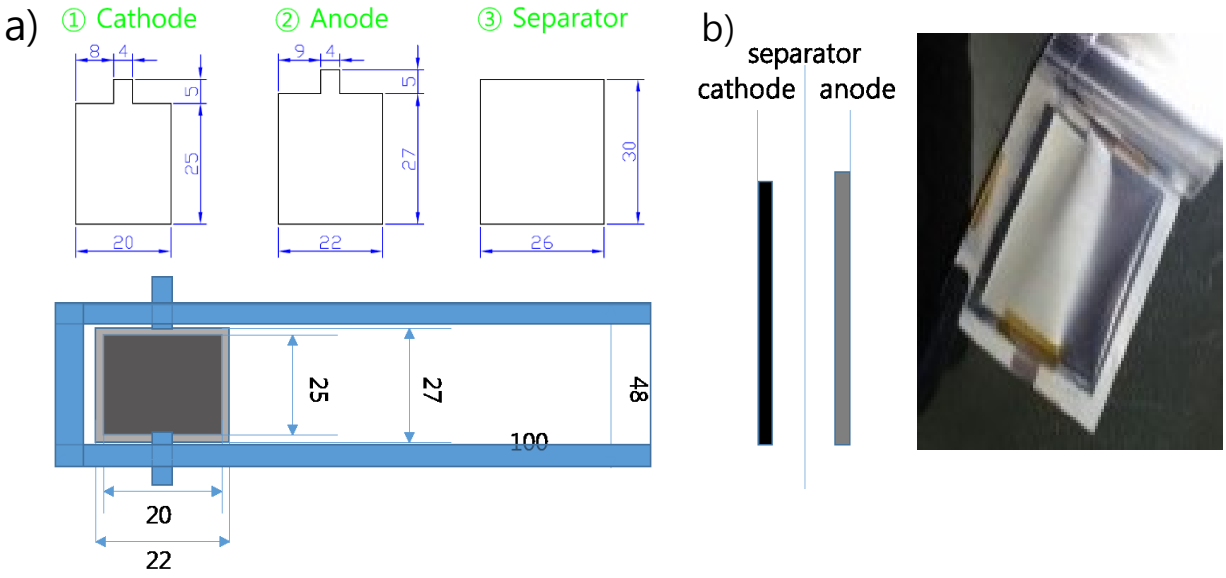

Figure 17. a) Pouch type full cell design. The standard of cathode electrode is 20.0mm x 25.0mm and that of anode is 22.0mm x 27.0mm. Separator size is 26.0mm x 30.0mm. The whole pouch size is 48.0mm x 100.0mm. b) Images of one-stack type pouch full cell.

The electrochemical performances were conducted via coin-type half-cell (2032R type) and pouch type full-cell. The cathode electrode were composed of 96wt% active materials which were commercial and prepared powder, respectively, 2wt% Super P carbon black as conduct material, 2wt% polyvinylidene fluoride(PVdF) binder. N-methyl-2-pyrrolidone(NMP) was used as a solvent to coating the electrode on Al foil, and then it dried at 120℃ for 1h. Used electrolyte was 1.15M LiPF6 with ethylene carbonate (EC) /dimethylene carbonate (DMC)/ diethylene carbonate (DEC) in 3:4:3 volume ratio (PANAX ETEC Co. Ltd., Korea). The active material loading level was 15mg cm^{-2}. All the half cells were assembled in a dry argon atmosphere globe box.

The half cells contains a cathode electrode and a lithium metal as an anode, separated by porous polypropylene film.[43] All electrochemical tests were conducted on WBCS-3000 (WonATech Co.) Galvanostatic charge and discharge test was performed between 4.3V and 3.0V (vs. Li/Li^+) at 25℃. The entire cells were galvanostatically charged to 4.3V at 0.1C rate, and kept 4.3V until the current reached to 0.05C rate, and then discharged to 3.0V at 0.1C rate.

Charge/discharge rate test was carried out from 0.5C to 5C and recovered to 0.5C, 3 cycles for each rate, respectively.

The galvanostatic intermittent titration technique (GITT) was employed at a constant current pulse of 15.0mA g^{-1}(=0.1C rate) for 1h, and then an open-circuit stands for 3h to relax the cell voltage to the steady state. The cells were galvanostatically charged and discharged at 0.1C rate at the voltage range of 3.0V to 4.3V (vs. Li/Li^+)

The whole full cell assembly was carried out in dry room, cell type was pouch one. The cathode loading was 15.9mg cm^{-2} (active material: 15.3mg cm^{-2}) and that of anode was 7.4mg cm^{-2} (Active material: 7.1mg cm^{-2}), N/P ratio is 1.12. The cathode electrode composition is same as that of half cells. The anode electrode is consisted of 96wt% of natural graphite active material, 1wt% of Super P carbon black conduct material, 1.5wt% of SBR and 1.5wt% of CMC. The amount of injected electrolyte was 0.3cc, about 0.36g for each cells. As shown in figure 17. a), the size of cathode is 5cm^2, anode is 5.94cm^2, separator is 7.8 cm^2. It is one-side stack type cell as shown in figure 17.b).

All electrochemical tests of full cell also were conducted on WBCS-3000 (WonATech Co.). Galvanostatic charge and discharge test was performed between 4.2V and 3.0V (vs. Li/Li^+) at 25℃. The entire cells were galvanostatically charged to 4.2V at 0.1C rate, and kept 4.2V until the current reached to 0.05C rate, and then discharged to 3.0V at 0.1C rate. Charge/discharge rate test was carried out from 0.5C to 3C and recovered to 0.5C, 3 cycles for each rate, respectively. In addition, DC-IR was measured to check the resistance and power of the cells.

2.3 Instrumental measurement

The crystalline phase of samples was identified by powder X-ray diffractometer (XRD, D/MAX-2200V, Rigaku) using Cu Ka radiation. The morphology of commercial and prepared powders was examined using scanning electron microscopy (SEM, S-4800, HITACHI). The cross sectional image of each sample was taken by focused ion beam (FIB, Quanta 3D FEG, FEI).

For BET and tab density measurement to figure out surface area of difference between each sample, Brunauer–Emmett–Teller (BET) method using an automatic surface analyzer (BET, Tristar II plus, Micromeritics). Tap density was obtained from envelope density analyzer (GeoPyc 1360, Micromeritics).

The electrochemical impedance spectroscopy (EIS) of 2032R coin-type half-cells were performed from 0.01 to 250kHZ frequency using electrochemical interface system (IVIUM) at SOC 100%, fully charged to 4.3V via constant current mode at 0.1C rate after formation test. To figure out activation energy from log scale Arrhenius plot, it undergoes the temperature change from 25℃ to -5℃ with 5℃ decrement scale in the low temperature controlled chamber. The impedance data were analyzed using ZView software.

III. Result and Discussions

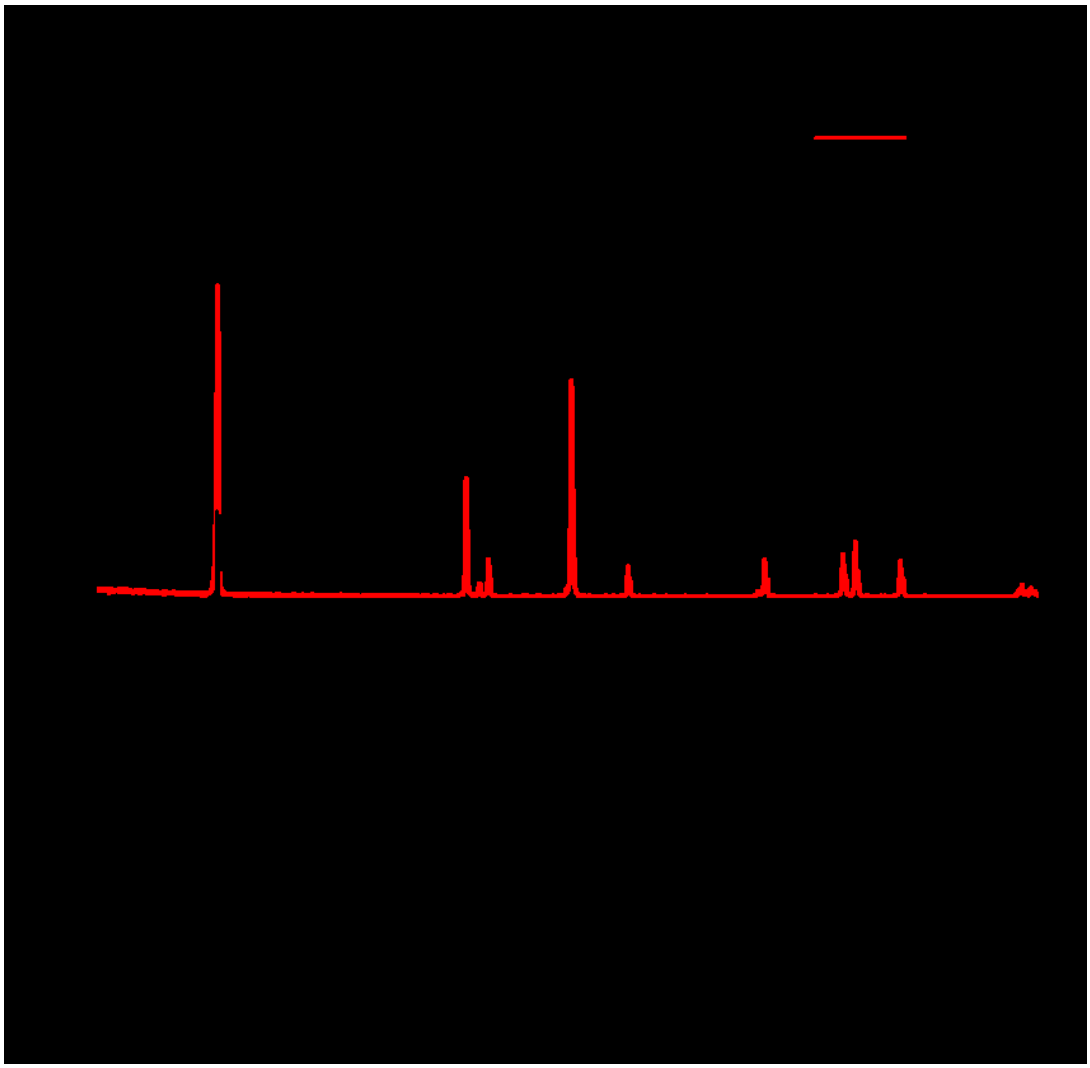

Figure 18. X-ray diffraction patterns for Bare $LiCoO_2$ (BLCO) and Spray-dried $LiCoO_2$ (SLCO).

Sample	I(003)/I(104)	FWHM	a (Å)	c (Å)	c/a ratio
BLCO	**2.19**	**0.1071**	**2.817**	**14.057**	**4.99**
SLCO	**1.62**	**0.1112**	**2.817**	**14.051**	**4.99**

Table 3. Characterization of Samsung Bare $LiCoO_2$ and Spray Bare $LiCoO_2$.

Figure 18 shows the XRD patterns of typical bare $LiCoO_2$ which has single crystal phase (denoted as BLCO) and spray-dried $LiCoO_2$ synthesized via sol-gel method (denoted as SLCO). All peaks exhibited a well-defined layered structure of space group $R\bar{3}m$ without any impurities. There were no particular differences between two samples peaks except I(003)/I(104) ratio. The intensity ratio I(003)/I(104) of BLCO was 2.19, that of SLCO was 1.62, respectively. The SLCO was calcinated at 900℃ during final process, so (003) layer were less developed compared to general $LiCoO_2$ which calcinated at 1000℃. Furthermore, the large surface area of SLCO causes more cation disordering at surface than BLCO, hence the peak ratio was lower. The lattice parameter a (2.817Å) was same on the both samples, *c* was slightly different, BLCO was bigger as 14.057Å compared to 14.051Å of SLCO. The ratio of a-axis and c-axis was 4.99 which represented the well-defined layered structure of high-temperature synthesized $LiCoO_2$.

The surface morphologies of each sample, BLCO, SLCO were confirmed by SEM, displayed on figure 19. The BLCO is consisted of two different-sized particles, so called bimodal. The large particles size of BLCO is around 15-20μm and that of small one is 2~3 μm. It has rocklike shape and dense morphology. On the contrast, the surface morphology of SLCO was spherical and porous with secondary particle size of approximately 15~20 μm in diameter. The SLCO secondary particles were composed of primary particles which size was around 1~1.5 μm. Cross sectional images of two samples were taken by FIB. As shown in figure. 19 (e) and (f), BLCO had dense inner connection because it is a single crystalline, while SLCO exhibited porous inner morphology. The EDX analysis results of BLCO and SLCO were exhibited in figure 20. The cobalt is well distributed in overall particles. The tap density of BLCO and SLCO were 2.7g/cc and 2.2g/cc, respectively. m

	BET(m^2/g)	Tap density (g/cc)	Pellet density (g/cc)
BLCO	0.27	2.8	4.0
SLCO	0.57	2.2	3.6

Table 4. Characteristic properties of BLCO and SLCO such as BET, tap density, and pellet density.

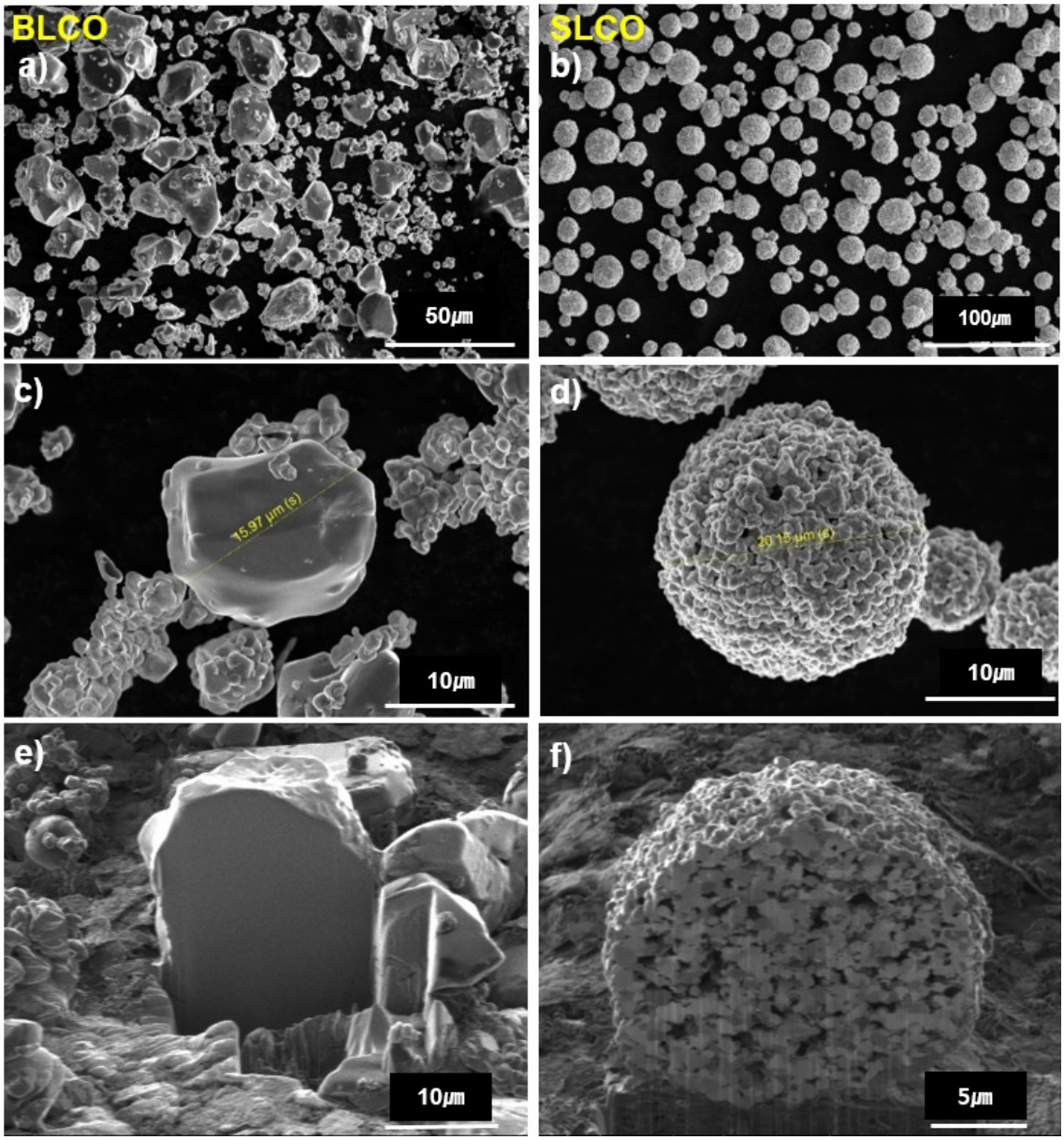

Figure 19. SEM images of (a) BLCO (low magnified image), (b) SLCO (low magnified image), (c) BLCO, (d) SLCO. Cross sectional FIB image of (e) BLCO, (f) SLCO.

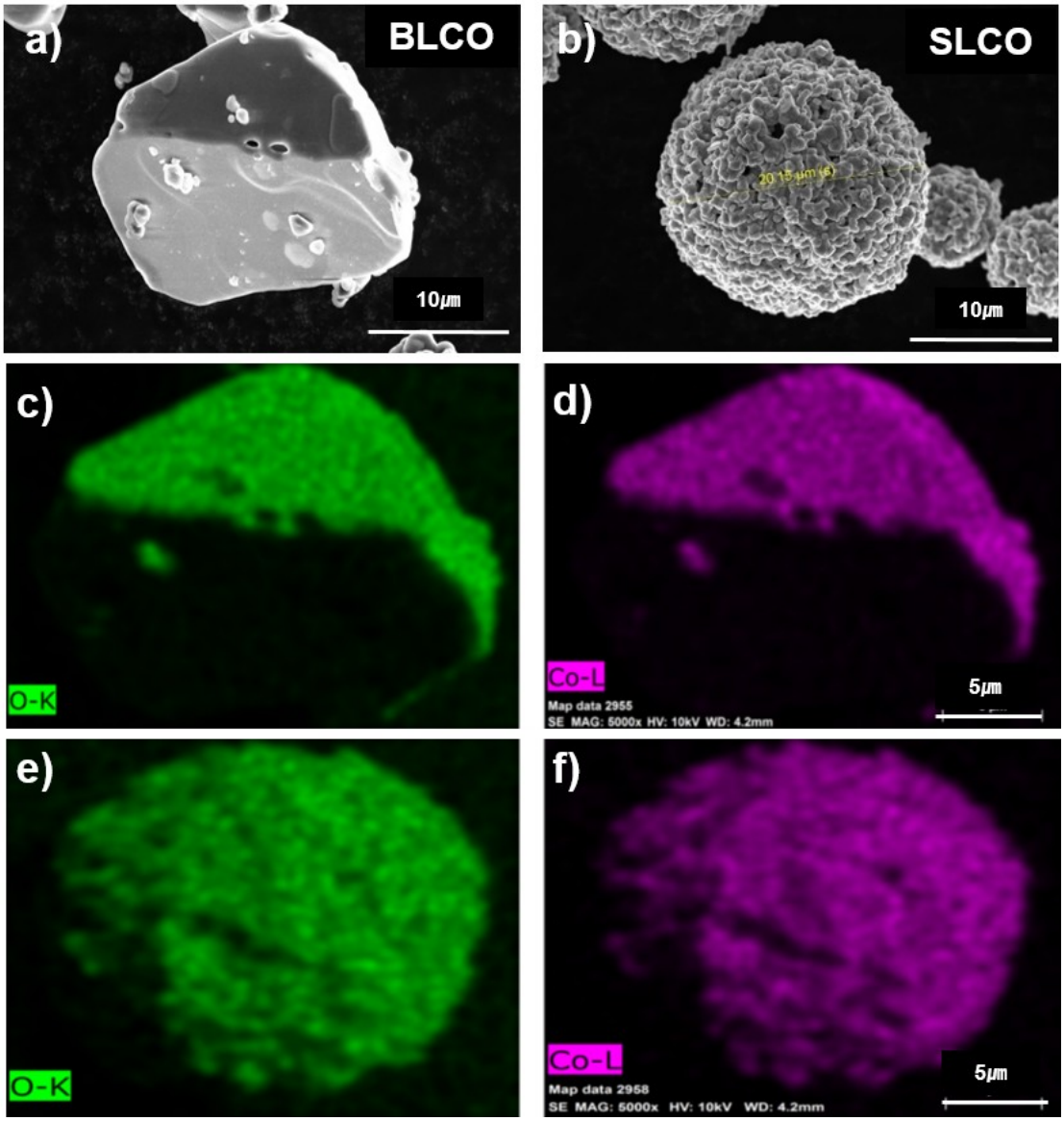

Figure 20. SEM images of BLCO, SLCO and EDX mapping for Co, O.

The first cycle charge and discharge voltage profiles of BLCO and SLCO are shown in figure 21. The half coin cell (2032R) were charged at 0.1C rate (1C = 150mAg^{-1}) until reached to 4.3V and maintained at the voltage till current decreased to 0.05C rates, then discharged at 0.1C rate to 3.0C at 25 ^{o}C. The discharge capacity of BLCO and SLCO were 163.7 and 165.6mAhg^{-1} and the coulombic efficiency of BLCO and SLCO were 97.2% and 96.9%, respectively. The discharge capacity of SLCO was smaller than that of BLCO since it has porous structure leading to large surface area, which forms abundant amount of SEI layer. Therefore, it has bigger irreversible capacity. Moreover, the capacity of SLCO from constant voltage mode was quite lower than that of BLCO. The capacity from constant voltage mode is correlated with the overpotential. It inferred the SLCO electrode has lower overpotential than BLCO one.

Figure 22 displays a) charge rate capabilities of BLCO and SLCO at 0.5C, 1C, 2C, 3C, 5C and 0.5C (recovery) rates during cycling in half coin cell. Discharge rate was fixed at 0.5C rate at 25℃. The charge voltage profiles of BLCO and SLCO at each C-rate were shown in figure 22 b) and c), respectively. Charge rate capacity retention of SLCO was higher than that of BLCO. Especially over the 3C rate, it reveals a huge disparity as more than 10% in retention compared with capacity at 0.5C rate. At 3C rate, the charge capacity retention of BLCO was 64.2%, while that of SLCO was 86.6%. Furthermore at 5C, BLCO shows only 6% capacity retention whereas SLCO does 47.5%. The reason why capacity retention gap between BLCO and SLCO increased as the rate goes higher comes from the surface area difference which leads to capability to generate more Li+ ion diffused out to electrolyte.

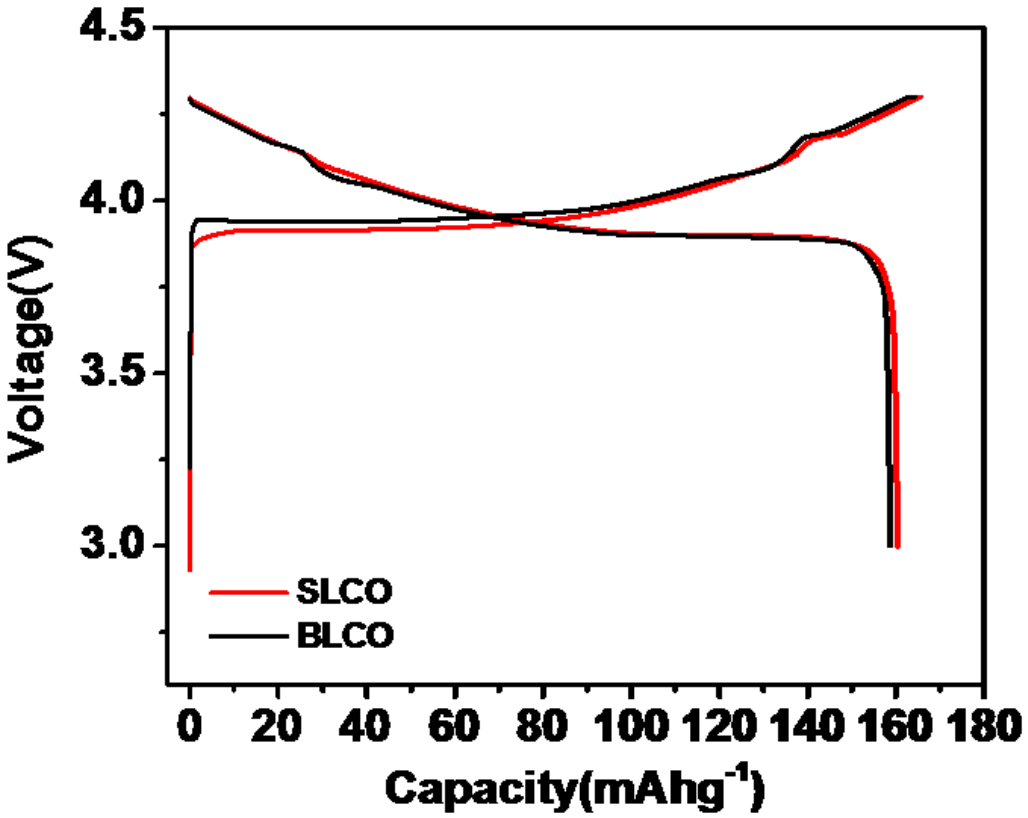

Figure 21. First formation charge and discharge profiles of BLCO (black) and SLCO (red) in half cells performed between 3.0-4.3V at 0.1C rate, 25 °C.

	Charging Capacity(mAh /g)	Discharging Capacity(mAh /g)	Coulombic Efficiency(%)
BLCO	163.7	159.2	97.2
SLCO	165.6	160.4	96.9

Table 5. Charging/discharging capacity and coulombic efficiency of BLCO and SLCO at 0.1C rate.

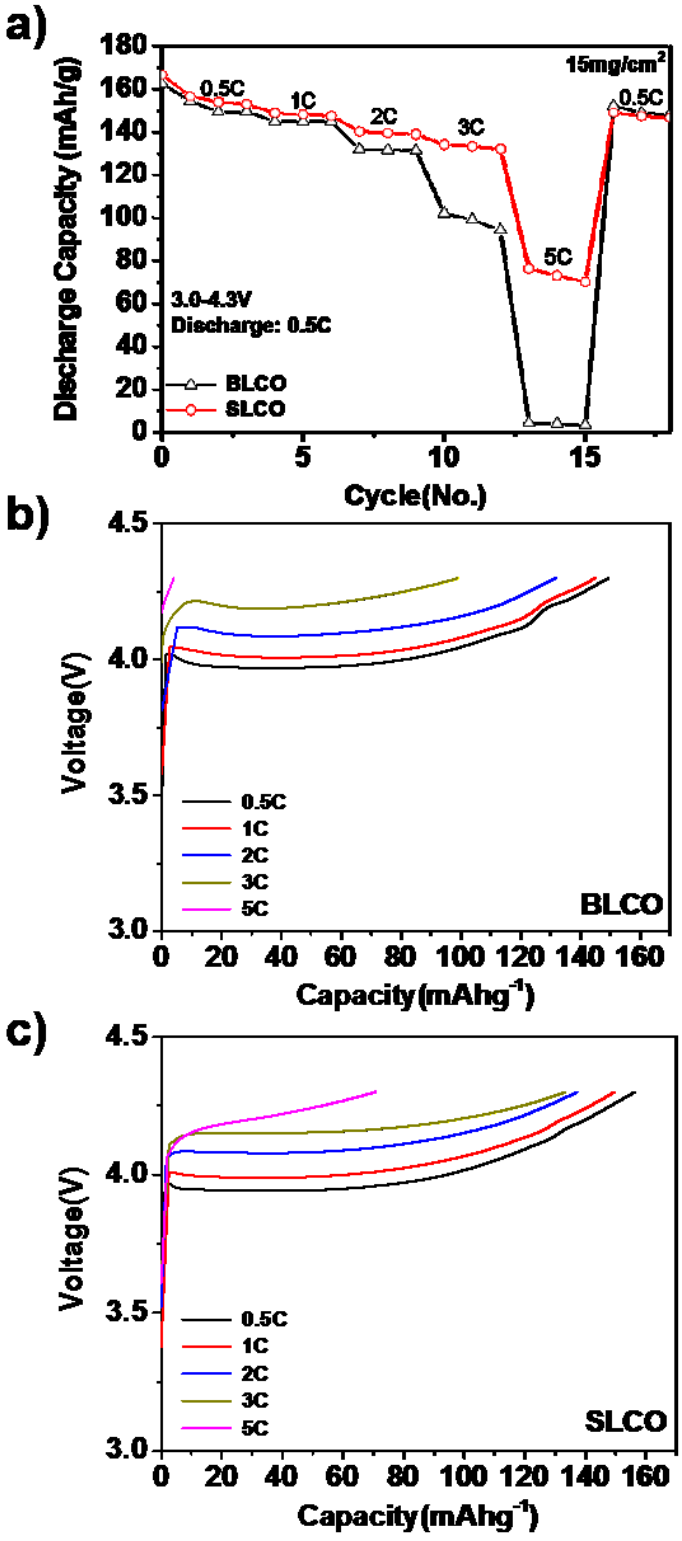

Figure 22. (a) Charge capacity retention of BLCO and SLCO electrodes as a range of various from 0.5 C (78 mA g^{-1}) to 5C (0.78 A g^{-1}) rate between 3.0 and 4.3 V at 25°C in coin half cells. The discharge current was fixed at 0.5 C. Charge voltage profiles of (b) BLCO and (c) SLCO. All the charge procedure were conducted on constant current mode.

vs. 0.5C capacity	1C	2C	3C	5C	0.5C(rec)
BLCO	94.0%	85.3%	64.2%	6.0%	96.4%
SLCO	96.3%	90.7%	86.6%	47.5%	95.8%

Table 6. Charge capacity retention of BLCO and SLCO vs 0.5C rate capacity in half coin cells.

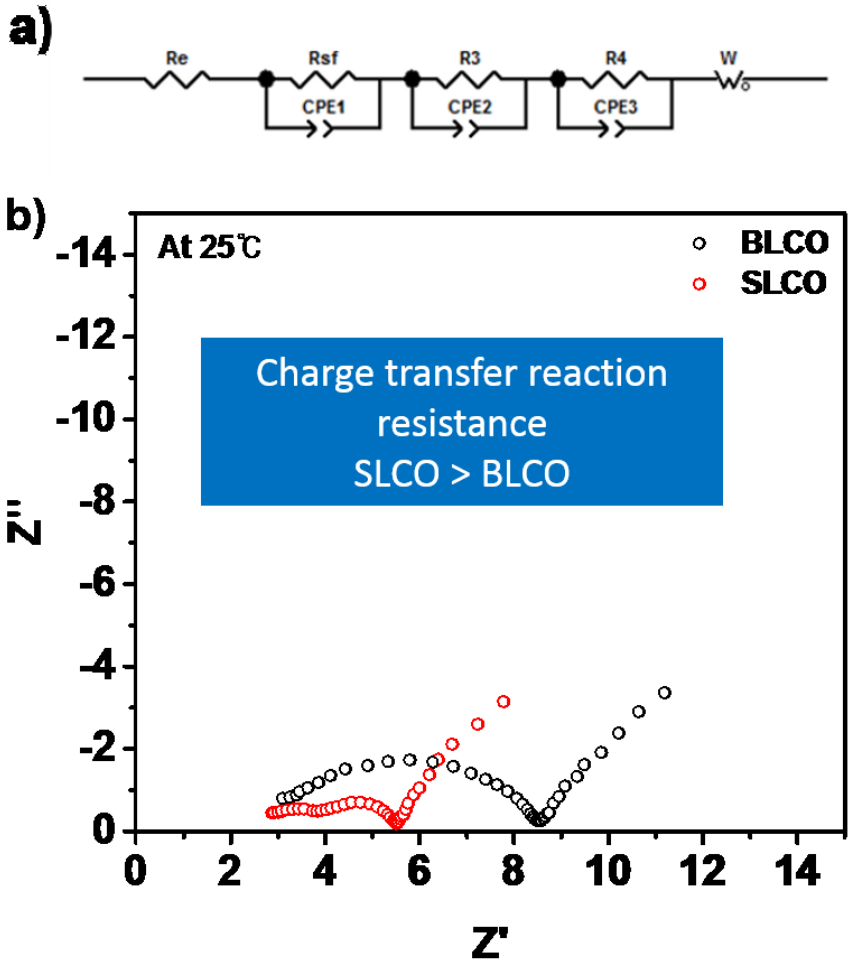

Figure 23. (a) The proposed equivalent circuit used for analyzing the impedance patterns. Nyquist plot for (b) BLCO and SLCO in regard to after formation.

An electrochemical impedance spectroscopy (EIS) analysis (shown in figure 23) was conducted to confirm the reason why the SLCO had better rate capability performance than the BLCO. In advance carry out the EIS analysis, the coin type half cells were charged and discharged from 3.0V to 4.3V at 0.1c rates, 25℃, as a first formation activation. Then it was charged again to 4.3V with same rates and temperature to analyze cell impedance at SOC 100% in this case. Figure 22 a) displays the equivalent circuit. The impedance pattern related to electronic resistance (R_e), SEI resistance + surface resistance ($R_{surface}$), Charge transfer resistance (R_{ct}) and Warburg impedance. Figure 23 b) shows the Nyquist plot of two sample after first and fully charged at 0.1C. The total impedance of BLCO was almost two times as big as that of SLCO. This result stems from surface area difference which correlated to the charge

transfer reaction. If surface area is larger, charge transfer reaction could be occur faster, but at the same time SEI layer forming is enlarged. In this case, fast charge transfer reaction effected mainly compared to SEI resistance.

Figure 24 (a) and (b) indicates the equivalent circuit of the impedance results with electronic resistance (R_e), SEI resistance + surface resistance($R_{surface}$), Charge transfer resistance (R_{ct}) and Warburg impedance, showing typical Nyquist plots of the BLCO and SLCO at different temperature from 25 ^{o}C to -5 ^{o}C. As the temperature decreased, total impedances of three electrode steeply increased the other way. Even though it is very difficult to identify each of the above resistance value from the overlapped semicircles in the middle frequency region, it is obvious that the total impedance of the SLCO is lower than that of the BLCO at any temperatures. The smaller semicircle of SLCO can be explained by adequate cation disordering at surface region to occur 'pillar effect', which prevent another side effect at surface.

In addition, in figure 24 (c), we plotted the activation energies for charge transfer reaction for each samples. The activation energies (Ea) for charge transfer were calculated from temperature dependencies of EIS results by using Arrhenius equation which is described below

$$k = \mathrm{A} \cdot exp\left(-\frac{Ea}{RT}\right)$$

(k= rate constant of reaction, A is pre-exponential factor, R is gas constant, and T is absolute temperature.)

The values of BLCO and SLCO were 48.7 and 38.5 kJ mol^{-1}, respectively. The one of factor of rate capability is the charge transfer reaction. The lower activation barrier indicates a higher charge transfer reaction kinetics in SLCO.

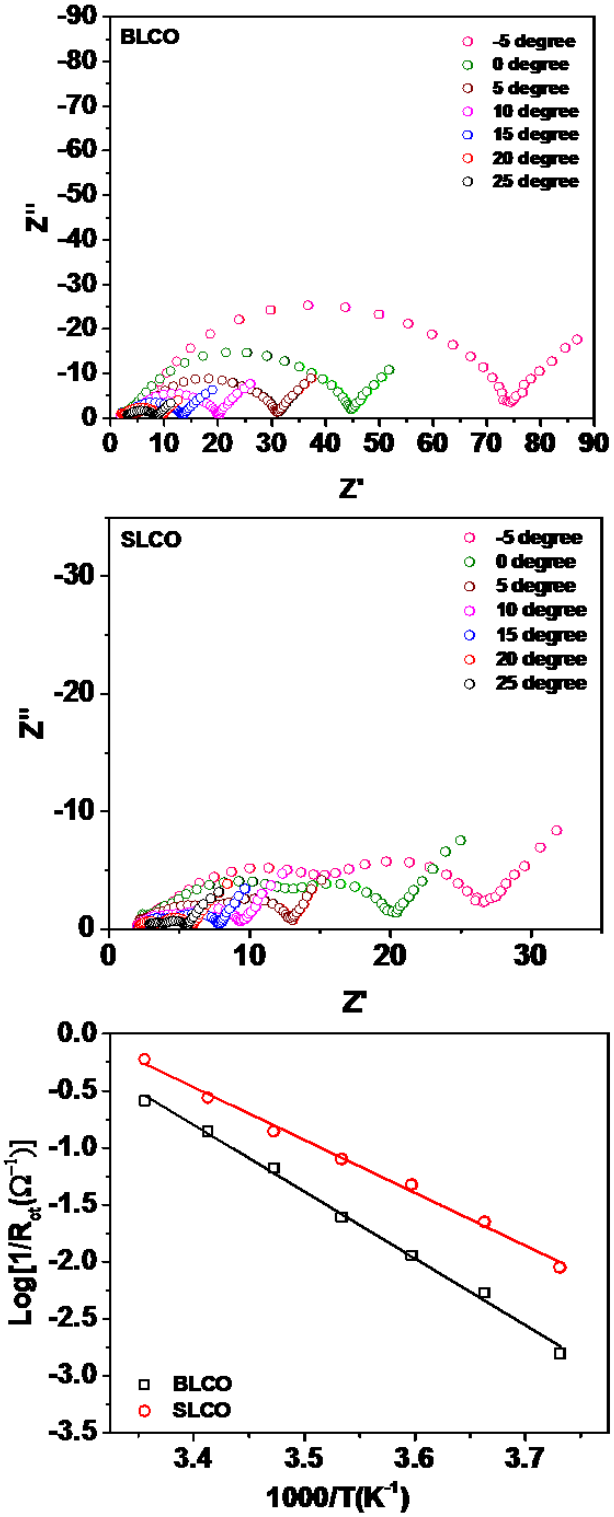

Figure 24. Nyquist plot of (a) BLCO, (b) SLCO as a function of temperatures from 25°C to -5°C with measurement of 5°C amount of interval. (c) Arrhenius plot of the charge-transfer reaction for BLCO and SLCO.

Not only charge transfer reaction influences to the higher rate capability, but also it is affected by polarization can be described as sum of ohmic potential and IR drop. The polarizations of those two electrode, BLCO and SLCO, were measured by means of galvanostatic intermittent titration technique, denoted as GITT.[44] Figure 25 exhibits GITT measurement result during charge from 3.0V to 4.3V at 0.1C rate and 1C rate, respectively. The temperature was 25°C. The constant current of 0.1C rate (15.0mAhg^{-1}) for 6 minutes and rest for 3 hours to relax the cell voltage were alternately applied for GITT measurement during charge (Figure 25 (a)). Likewise, the constant current of 1C rate (150mAhg^{-1}) for 1 hour and rest for 3 hours as same reason during charge (Figure 25 (b)). As shown in figure 25 (c) – (f), the composite electrodes exhibited quite lower overpotential throughout the entire stoichiometric state of 1-δ. The real properties of the electrodes and materials used for battery are not equal to that of theoretical value.

Generally, the polycrystalline structure has a lot of grain boundary, thus the electron conduction from inside from inside of particle takes relatively long time. But, in terms of the Li+ ion conductivity and movement of Li+ is easier due to its shorter diffusion length and larger surface area to move out from inside between electrolyte and particles. Also, IR-drop of BLCO is bigger than that of SLCO against to expectation, since electron conduction is usually better in single crystal. Also the sufficient amount of conductive agent is not added in electrode due to concern for decreasing cell capacity even though it is known that larger amount of conductive carbon results in higher rate capability. Therefore, we supposed that the disordering at the surface of polycrystalline might play a role as “pillar” which prevent further side reaction due to the larger surface area, as the reason why. To figure it out more precisely, we need a further analysis such as TEM. Also, relaxation time should be much longer to find out exact rate determine steps.

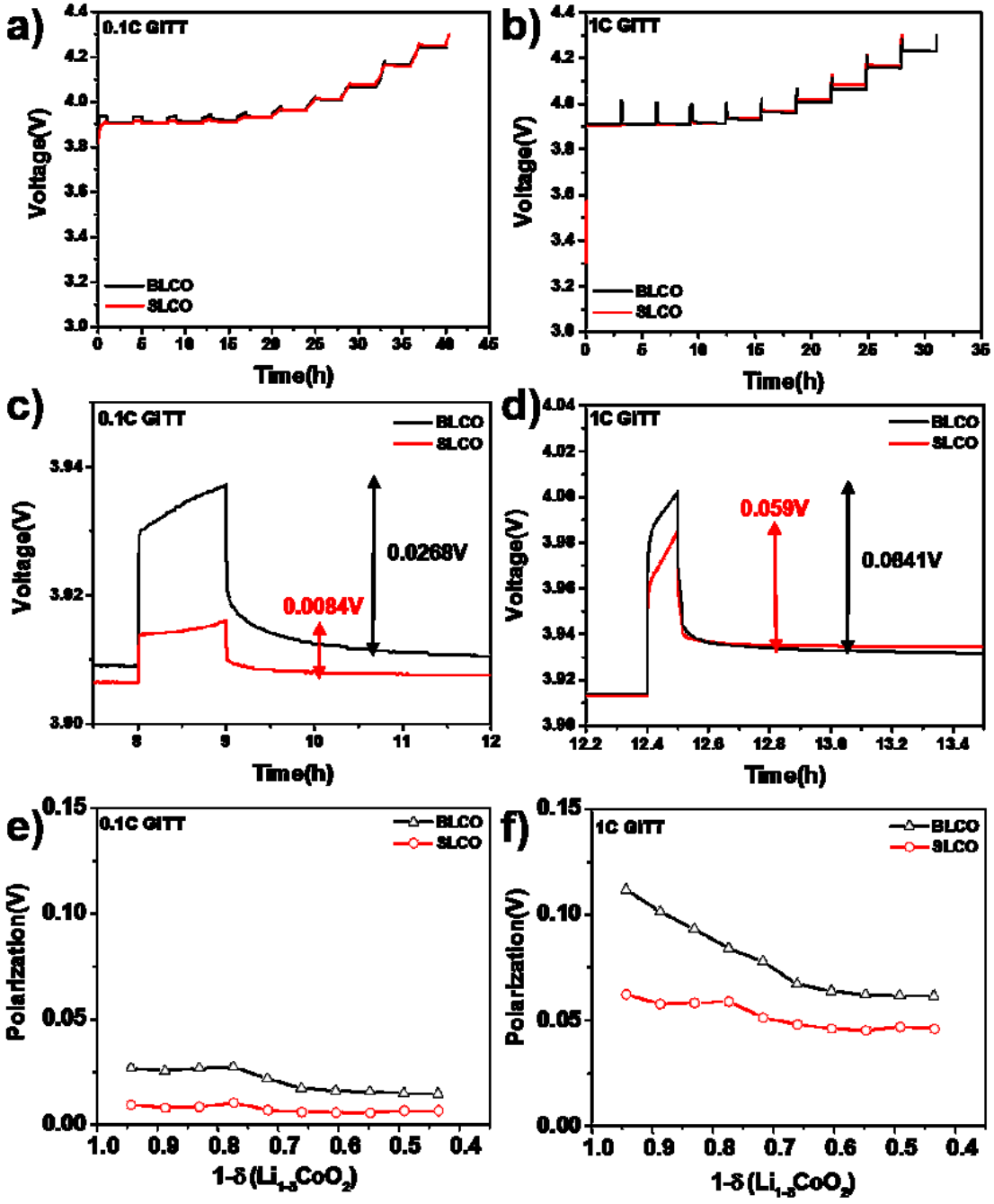

Figure 25. GITT potential response during charge (a) at 0.1C rate and (b) at 1C rate. (c) and (d) are expanded images of the regions in (a) and (b), respectively. Polarization of BLCO and SLCO during charge (e) at 0.1C rate and (f) at 1C rate.

Figure 26 displays the cyclic voltammetry (CV) analysis results of BLCO and SLCO. The scan rate was applied as a range of 0.01mV/sec to 1mV/sec (0.01, 0.03, 0.05, 0.1, 0.3, 0.5, 1mV/sec). Cyclic voltammetry electrochemical test is involved in potential sweep methods. Generally since the electrode which has small area are used, it could be assumed there are no change of bulk concentration C_O* and C_R*, respectively. Furthermore, the migration of ion can be ignored. So mass transfer factor only depends on linear diffusion. CV method used to figure out the factor correlated to charge transfer, mass transfer and reaction mechanism in ordinary.

The peak current can be expressed as following equation, called Randles-Sevick Equation. The coefficient(2.69×10^5) comes from the F=96485C/mol, R=8.314J/mol K and T = 298K.

$$i_p = \left(2.69 \times 10^5\right) n^{3/2} A D_{Li^+}{}^{1/2} C v^{1/2}$$

(A = active site surface area; cm2, C = bulk concentration: mol/cm3, v =scan rate; mV/sec, i_p = peak current; mA)

Using above equation, we can plot the peak current as a function of scan rate as shown in figure 26(b) and (d). The slope of those graphs means the multiply of each coefficient. Among them, Li+ ion diffusion coefficient and bulk concentration are intrinsic factor of same composition material, it can be fixed as same value. The real factor affect to the peak current magnitude in this case is active site surface area, A. Lots of cases assume the A as electrode area, but actually the real part to participate in the activation is different for each sample. Therefore, the real active site of SLCO is larger than that of BLCO. This conclusion deducted from the comparison of the slope magnitude at figure 26(b) and (c). Through linear fitting at each case, SLCO exhibit steep slope compared to BLCO.

In figure 27, the electric double layer capacitance (EDLC) analysis was exhibited as a function of various scan rate from 0.01mV/sec to 1mV/sec between 2.5V to 3.0V The temperature was 25 ^oC. It can be intuitionally recognized from the gap between surrounded

areas at each scan rate. The integral of the SLCO is much bigger than that of BLCO, which implied the surface area of the SLCO was larger.

While the CV involves the both faradaic and non-faradaic reaction region, electric double layer capacitance analysis only focused on non-faradaic reaction. Before faradaic reaction (denoted as redox reaction) occur, electron usually accumulated on the surface of electrode until its energy reached to LUMO of reactants. With those reasons, as can be seen in below equation, the electric double layer capacitance is proportional to the surface area.

$$C = \frac{\varepsilon A}{d}.$$

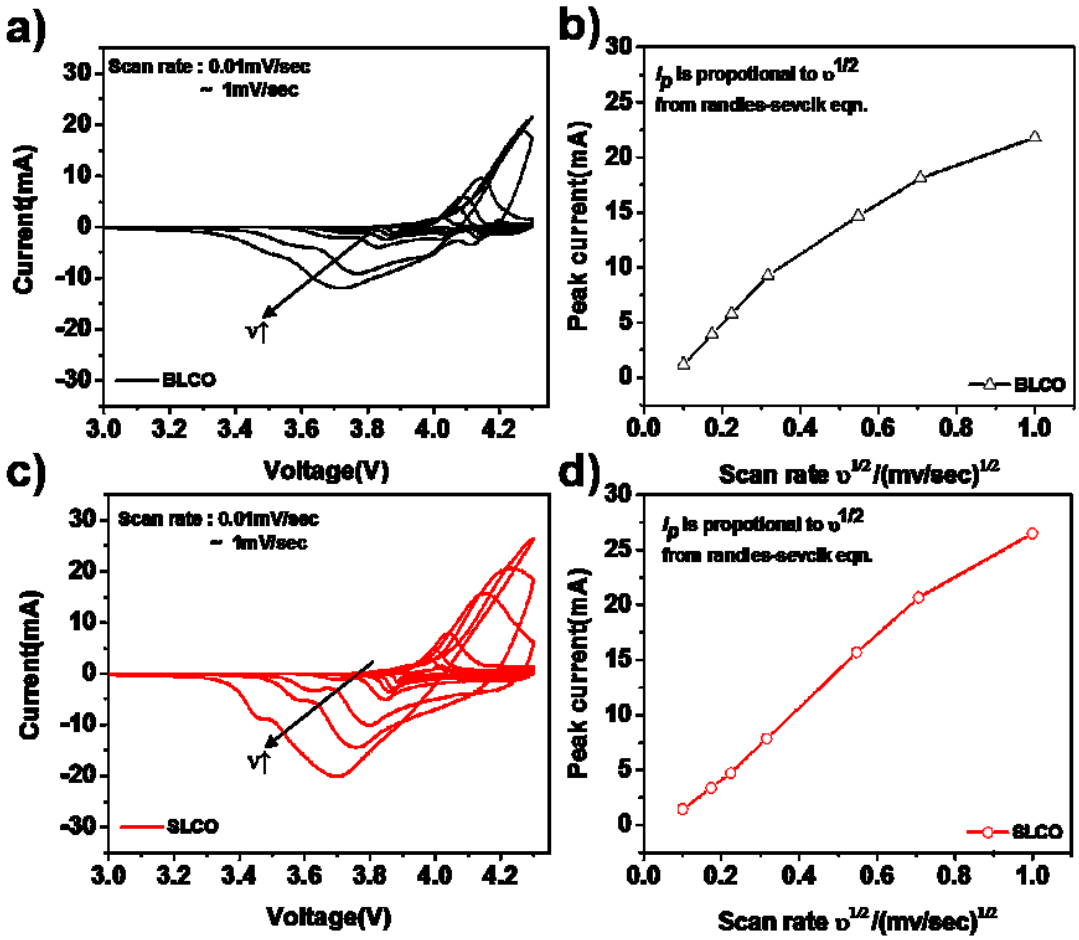

Figure 26. Cyclic voltammetry analysis of (a) BLCO and (c) SLCO as a function of various scan rates from 0.01mV/sec to 1mV/sec between 3.0 and 4.3V at 25 °C. The peak current i_p (mA) plot of (b) BLCO and (d) SLCO versus root squre of scan rate $v^{1/2}$ (mv/sec) $^{1/2}$.

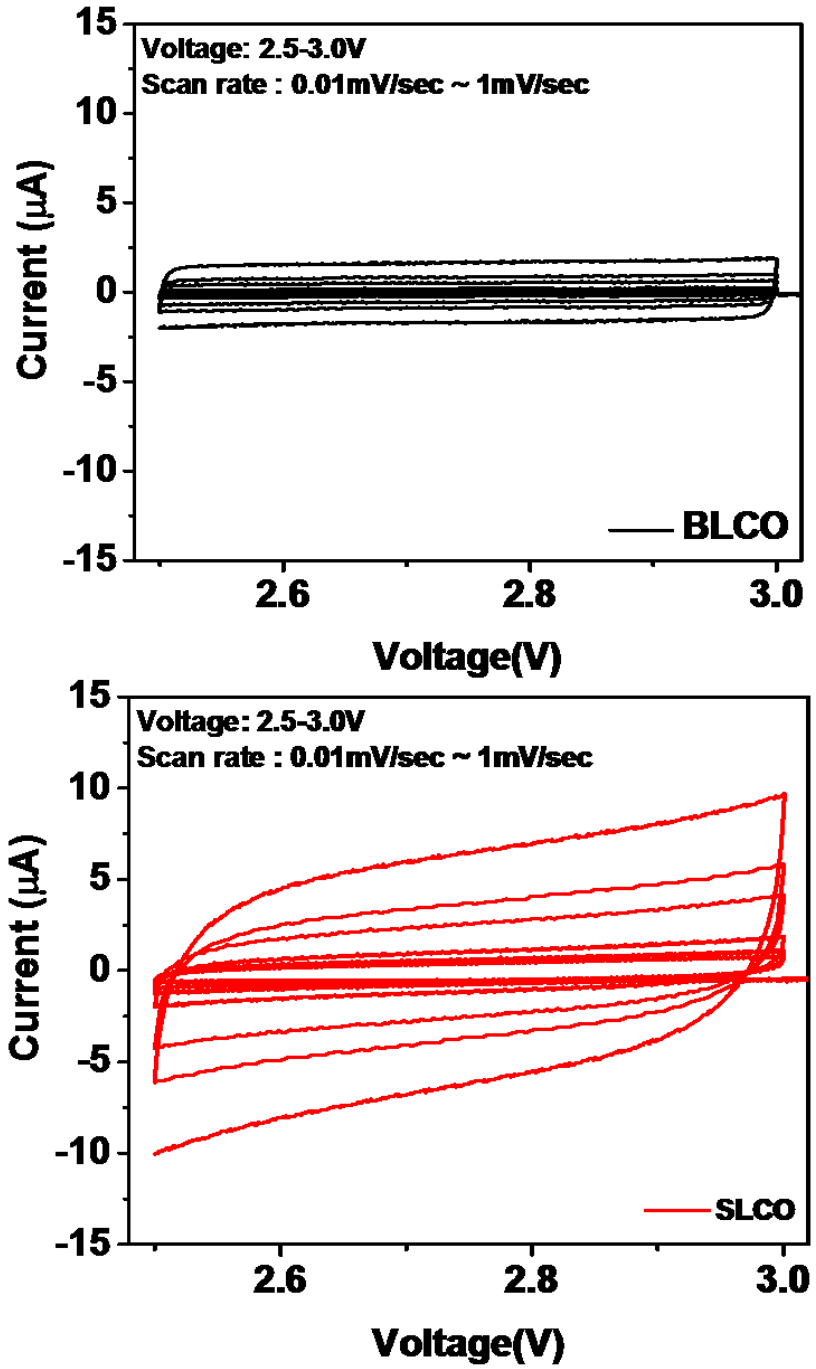

Figure 27. The electric double layer capacitance (EDLC) analysis as a function of various scan rate from 0.01mV/sec to 1mV/sec between 2.5V to 3.0V where the non-faradaic reactions occur. The temperature was 25 °C.

The first cycle charge and discharge voltage profiles of BLCO and SLCO full cells are shown in figure 28. The anode electrode was natural graphite called SG-17. Its theoretical reversible capacity was 360.0mAhg-1 and efficiency was 91.0%. The N/P ratio was 1.12 in both samples. The one-side stack type pouch full cells were charged at 0.1C rate (1C = 150mAg^{-1}) until reached to 4.2V and maintained at the voltage till current decreased to 0.02C rates, then discharged at 0.1C rate to 3.0C at 25 °C. The discharge capacity of BLCO and SLCO were 12.3 and 12.1mAh and the coulombic efficiency of BLCO and SLCO were both 90.9%. An evitable meager difference of loading caused slightly higher capacity of BLCO compared to that of SLCO in terms of absolute value of capacity. Moreover, the capacity of SLCO from constant voltage mode was quite lower than that of BLCO. The capacity from constant voltage mode is correlated with the overpotential. It inferred the SLCO electrode has lower overpotential than BLCO one.

Figure 29 exhibits a) charge rate capabilities of BLCO and SLCO at 0.5C, 1C, 2C, 3C, 5C and 0.5C (recovery) rates during cycling in one-side stack type pouch full cell. Discharge rate was fixed at 0.5C rate at 25℃. The charge voltage profiles of BLCO and SLCO at each C-rate were shown in figure 29 b) and c), respectively. Charge rate capacity retention of SLCO was higher than that of BLCO. Especially over the 3C rate, it reveals a huge disparity as more than 9% in retention compared with capacity at 0.5C rate. At 3C rate, the charge capacity retention of BLCO was 72.5%, while that of SLCO was 82.7%. Furthermore at 5C, BLCO shows 52.4% capacity retention whereas SLCO does 70.6%. The reason why capacity retention gap between BLCO and SLCO increased as the rate goes higher comes from the surface area difference which leads to capability to generate more Li+ ion diffused out to electrolyte. In addition, the capacity retention differed from half cells electrochemical test since the lithium metal reference electrode (which act as anode in half cell) is sensitive to amount of current applied to unit area. Hence, as the rate raised, especially at the 5C rate test, there was definite difference.

Furthermore, figure 30 shows the cycling performance as cycle retention. All cells were charged at 1C rates and discharged at 1C rates from 3.0V to 4.2V at 25 °C. The SLCO displayed better cycle retention of 96.3% than that of BLCO (85.1%) after 150cycles at 25 °C.

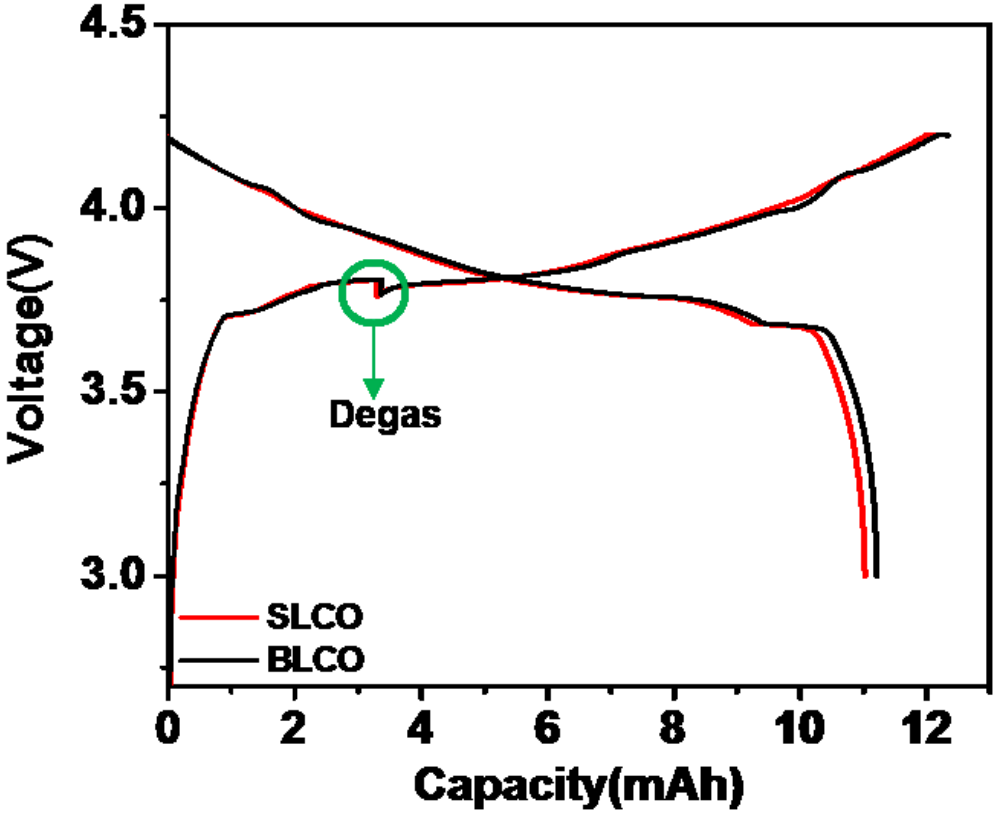

Figure 28. First formation charge and discharge profiles of BLCO (black) and SLCO (red) in one-side stack type pouch full cells performed between 3.0-4.2V at 0.1C rate, 25°C. The anode electrode was natural graphite, called SG-17.

	Charging Capacity(mAh)	Discharging Capacity(mAh)	Coulombic Efficiency(%)
BLCO	12.3	11.2	90.9
SLCO	12.1	11.0	90.9

Table 7. Charge capacity retention of BLCO and SLCO vs 0.5C rate capacity in one-stack type pouch full cells.

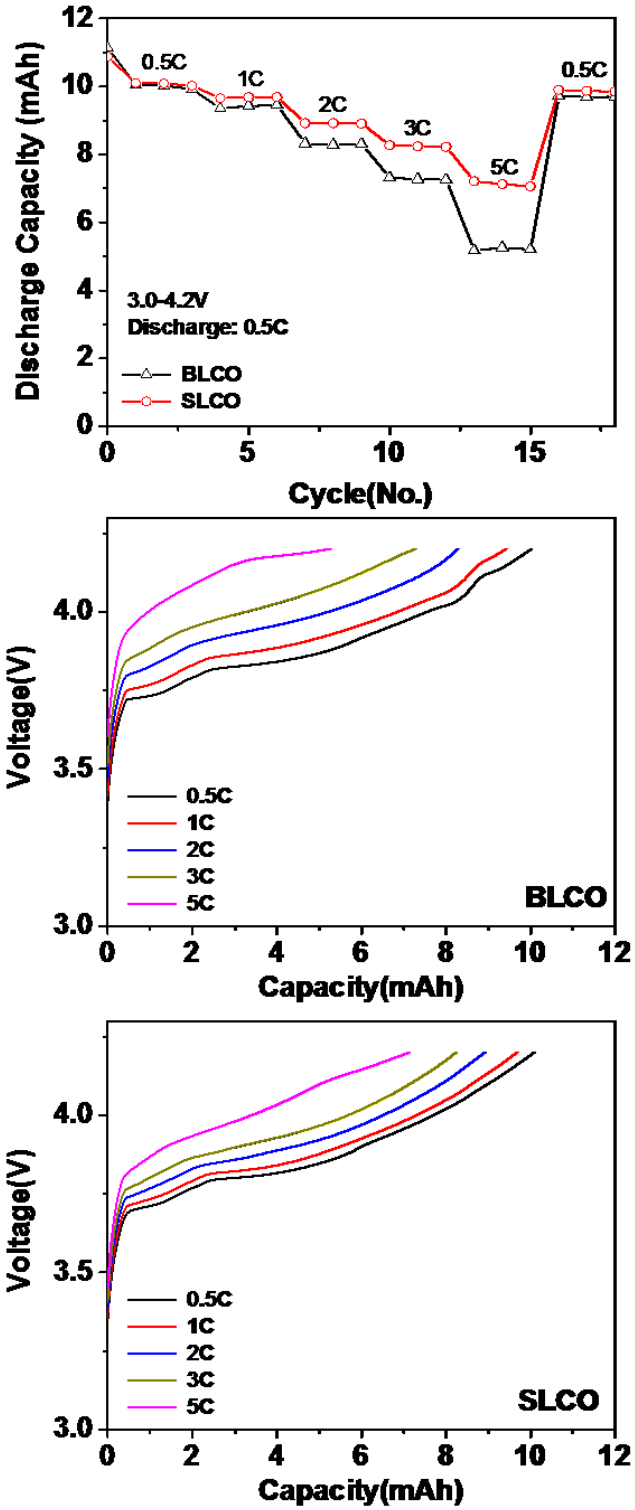

Figure 29. a) Charge capacity retention of BLCO and SLCO electrodes as a range of various from 0.5 C (5.5mA) to 5C (55mA) rate between 3.0 and 4.2 V at 25°C in pouch

full cells. The discharge current was fixed at 0.5 C. Charge voltage profiles of b) BLCO and c) SLCO. All the charge procedure were conducted on constant current mode.

vs. 0.5C capacity	1C	2C	3C	5C	0.5C(rec)
BLCO	94.0%	82.6%	72.5%	52.4%	96.6%
SLCO	96.0%	88.4%	81.7%	70.6%	97.8%

Table 8. Charge capacity retention of BLCO and SLCO vs 0.5C rate capacity in pouch type full cells.

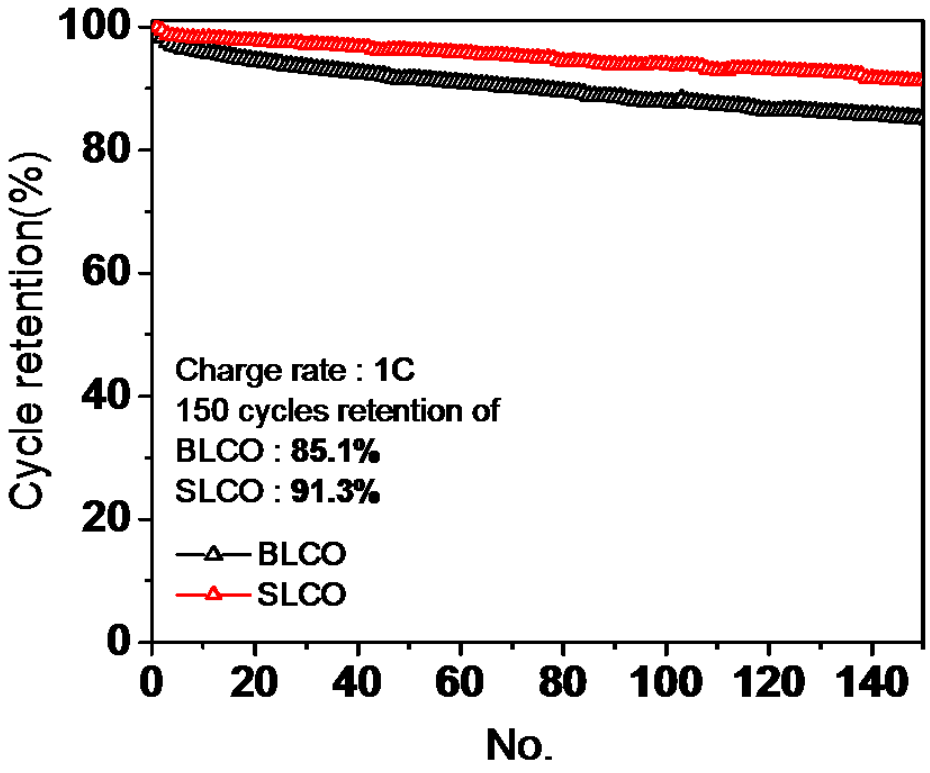

Figure 30. Cycle retention performance of BLCO and SLCO at 1C charge rate and 1C discharge rate in pouch type full cell at 25 °C.

IV. Conclusion

In summary, we successfully synthesized $LiCoO_2$ secondary particle with porous and spherical shape consisted of 1~1.5 ㎛ size primary particle. The newly developed material SLCO enhanced the rate capability as well as the cycle performance especially at full cells compared to those of single crystal bimodal type BLCO. Especially in full cell, they showed almost same coulombic efficiency and charge/discharge capacity. We can conclude that the surface area effect was the main reason to improve the rate performance from the physical properties and EDLC and cyclic voltammetry analysis. Furthermore, from the EIS analysis, the total impedance and especially the charge transfer resistance of BLCO is much bigger than that of SLCO, so the optimized size and morphology of SLCO were effective to enhance both of cyclic performance and rate capability.

If more treatment such as thin carbon coating or binding during the spary-drying procedure, it can be enhanced more in terms of electric connectivity and stability.

V. References

1. Kang, K.; Meng, Y. S.; Bréger, J.; Grey, C. P.; Ceder, G., Electrodes with high power and high capacity for rechargeable lithium batteries. *Science* **2006,** *311* (5763), 977-980.

2. Larcher, D.; Tarascon, J. M., Towards greener and more sustainable batteries for electrical energy storage. *Nat Chem* **2015,** *7* (1), 19-29.

3. Tarascon, J. M.; Armand, M., Issues and challenges facing rechargeable lithium batteries. *Nature* **2001,** *414* (6861), 359-367.

4. Dunn, B.; Kamath, H.; Tarascon, J.-M., Electrical energy storage for the grid: a battery of choices. *Science* **2011,** *334* (6058), 928-935.

5. Thackeray, M. M.; Wolverton, C.; Isaacs, E. D., Electrical energy storage for transportation—approaching the limits of, and going beyond, lithium-ion batteries. *Energy & Environmental Science* **2012,** *5* (7), 7854-7863.

6. Whittingham, M. S., Lithium batteries and cathode materials. *Chemical Reviews* **2004,** *104* (10), 4271-4301.

7. Joost, M.; Alexander, S., 17th International Meeting on Lithium Batteries. *Johnson Matthey Technology Review* **2015,** *59* (1), 56-63.

8. Ohzuku, T.; Ueda, A., Solid-State Redox Reactions of LiCoO2 (R3¯m) for 4 Volt Secondary Lithium Cells. *Journal of The Electrochemical Society* **1994,** *141* (11), 2972-2977.

9. Shao-Horn, Y.; Croguennec, L.; Delmas, C.; Nelson, E. C.; O'Keefe, M. A., Atomic resolution of lithium ions in LiCoO2. *Nature materials* **2003,** *2* (7), 464-467.

10. Mizushima, K.; Jones, P. C.; Wiseman, P. J.; Goodenough, J. B., LIXCOO2 "(OLESS-THANXLESS-THAN-OR-EQUAL-TO1) - A NEW CATHODE MATERIAL FOR BATTERIES OF HIGH-ENERGY DENSITY. *Materials Research Bulletin* **1980,** *15* (6), 783-789.

11. Sun, Y.-K.; Oh, I.-H.; Hong, S.-A., Synthesis of ultrafine LiCoO2 powders by the sol-gel method. *Journal of materials science* **1996,** *31* (14), 3617-3621.

12. Kim, J.; Fulmer, P.; Manthiram, A., Synthesis of LiCoO 2 cathodes by an oxidation reaction in solution and their electrochemical properties. *Materials research bulletin* **1999,** *34* (4), 571-579.

13. (a) Chen, J.; Wang, S.; Whittingham, M. S., Hydrothermal synthesis of cathode materials. *Journal of Power Sources* **2007,** *174* (2), 442-448; (b) Burukhin, A.; Brylev, O.; Hany, P.; Churagulov, B. R., Hydrothermal synthesis of LiCoO 2 for lithium rechargeable batteries. *Solid State Ionics* **2002,** *151* (1), 259-263.

14. Larcher, D.; Palacin, M.; Amatucci, G.; Tarascon, J. M., Electrochemically active LiCoO2 and LiNiO2 made by cationic exchange under hydrothermal conditions. *Journal of The Electrochemical Society* **1997,** *144* (2), 408-417.

15. (a) Gummow, R.; Thackeray, M.; David, W.; Hull, S., Structure and electrochemistry of lithium cobalt oxide synthesised at 400 C. *Materials research bulletin* **1992,** *27* (3), 327-337; (b) Nazri, G.-A.; Pistoia, G., *Lithium batteries: science and technology*. Springer Science & Business Media: 2008.

16. Shao-Horn, Y.; Hackney, S.; Kahaian, A.; Thackeray, M., Structural Stability of LiCoO 2 at 400° C. *Journal of Solid State Chemistry* **2002,** *168* (1), 60-68.

17. Chen, Z. H.; Dahn, J. R., Methods to obtain excellent capacity retention in LiCoO2 cycled to 4.5 V. *Electrochimica Acta* **2004,** *49* (7), 1079-1090.

18. Cho, J.; Kim, Y. J.; Kim, T. J.; Park, B., Zero-strain intercalation cathode for rechargeable Li-ion cell. *Angewandte Chemie-International Edition* **2001,** *40* (18), 3367-+.

19. Arai, H.; Hayashi, M., SECONDARY BATTERIES – LITHIUM RECHARGEABLE SYSTEMS – LITHIUM-ION | Positive Electrode: Lithium Cobalt Oxide A2 - Garche, Jürgen. In *Encyclopedia of Electrochemical Power Sources*, Elsevier: Amsterdam, 2009; pp 258-263.

20. Lu, X.; Sun, Y.; Jian, Z.; He, X.; Gu, L.; Hu, Y.-S.; Li, H.; Wang, Z.; Chen, W.; Duan, X., New Insight into the Atomic Structure of Electrochemically Delithiated O3-Li (1–x) CoO2 (0≤ x≤ 0.5) Nanoparticles. *Nano letters* **2012,** *12* (12), 6192-6197.

21. Amatucci, G.; Tarascon, J.; Klein, L., Cobalt dissolution in LiCoO 2-based non-aqueous rechargeable batteries. *Solid State Ionics* **1996,** *83* (1), 167-173.

22. Amatucci, G. G.; Tarascon, J. M.; Klein, L. C., CoO_2, The End Member of the Li_xCoO_2 Solid Solution. *Journal of The Electrochemical Society* **1996,** *143* (3), 1114-1123.

23. Gabrisch, H.; Yazami, R.; Fultz, B., Hexagonal to Cubic Spinel Transformation in Lithiated Cobalt Oxide: TEM Investigation. *Journal of The Electrochemical Society* **2004,** *151* (6), A891-A897.

24. Fu, L. J.; Liu, H.; Li, C.; Wu, Y. P.; Rahm, E.; Holze, R.; Wu, H. Q., Surface modifications of electrode materials for lithium ion batteries. *Solid State Sciences* **2006,** *8* (2), 113-128.

25. (a) Cho, J.; Kim, Y. J.; Park, B., Novel LiCoO2 cathode material with Al2O3 coating for a Li ion cell. *Chemistry of Materials* **2000,** *12* (12), 3788-3791; (b) Cho, J.; Kim, Y. J.; Park, B., LiCoO2 cathode material that does not show a phase transition from hexagonal to monoclinic phase. *Journal of The Electrochemical Society* **2001,** *148* (10), A1110-A1115.

26. Cho, J.; Kim, G., Enhancement of Thermal Stability of LiCoO2 by LiMn2 O 4 Coating.

Electrochemical and solid-state letters **1999,** *2* (6), 253-255.

27. Bard, A. J.; Faulkner, L. R.; Leddy, J.; Zoski, C. G., *Electrochemical methods: fundamentals and applications*. Wiley New York: 1980; Vol. 2.

28. Lee, M.-J.; Lee, S.; Oh, P.; Kim, Y.; Cho, J., High performance LiMn2O4 cathode materials grown with epitaxial layered nanostructure for Li-ion batteries. *Nano letters* **2014,** *14* (2), 993-999.

29. Zhao, J.; Wang, L.; He, X.; Wan, C.; Jiang, C., Kinetic investigation of LiCOO2 by electrochemical impedance spectroscopy (EIS). *Int. J. Electrochem. Sci* **2010,** *5*, 478-488.

30. Levi, M.; Salitra, G.; Markovsky, B.; Teller, H.; Aurbach, D.; Heider, U.; Heider, L., Solid-State Electrochemical Kinetics of Li-Ion Intercalation into Li1− x CoO2: Simultaneous Application of Electroanalytical Techniques SSCV, PITT, and EIS. *Journal of The Electrochemical Society* **1999,** *146* (4), 1279-1289.

31. Meyers, J. P.; Doyle, M.; Darling, R. M.; Newman, J., The impedance response of a porous electrode composed of intercalation particles. *Journal of The Electrochemical Society* **2000,** *147* (8), 2930-2940.

32. Li, C.; Zhang, H. P.; Fu, L. J.; Liu, H.; Wu, Y. P.; Ram, E.; Holze, R.; Wu, H. Q., Cathode materials modified by surface coating for lithium ion batteries. *Electrochimica Acta* **2006,** *51* (19), 3872-3883.

33. (a) Mladenov, M.; Stoyanova, R.; Zhecheva, E.; Vassilev, S., Effect of Mg doping and MgO-surface modification on the cycling stability of LiCoO2 electrodes. *Electrochemistry Communications* **2001,** *3* (8), 410-416; (b) Myung, S. T.; Kumagai, N.; Komaba, S.; Chung, H. T., Effects of Al doping on the microstructure of LiCoO2 cathode materials. *Solid State Ionics* **2001,** *139* (1-2), 47-56; (c) Reimers, J.; Dahn, J.; Von Sacken, U., Effects of impurities on the electrochemical properties of LiCoO2. *Journal of The Electrochemical Society* **1993,** *140* (10), 2752-2754.

34. (a) Gaberscek, M.; Dominko, R.; Jamnik, J., Is small particle size more important than carbon coating? An example study on LiFePO4 cathodes. *Electrochemistry Communications* **2007,** *9* (12), 2778-2783; (b) Okubo, M.; Hosono, E.; Kim, J.; Enomoto, M.; Kojima, N.; Kudo, T.; Zhou, H.; Honma, I., Nanosize effect on high-rate Li-ion intercalation in LiCoO2 electrode. *Journal of the American Chemical Society* **2007,** *129* (23), 7444-7452; (c) Jo, M.; Hong, Y.-S.; Choo, J.; Cho, J., Effect of LiCoO2 cathode nanoparticle size on high rate performance for Li-ion batteries. *Journal of The Electrochemical Society* **2009,** *156* (6), A430-A434; (d) Jo, M.; Jeong, S.; Cho, J., High power LiCoO 2 cathode materials with ultra energy density for Li-ion

cells. *Electrochemistry Communications* **2010,** *12* (7), 992-995.

35. Cao, Q.; Zhang, H. P.; Wang, G. J.; Xia, Q.; Wu, Y. P.; Wu, H. Q., A novel carbon-coated LiCoO2 as cathode material for lithium ion battery. *Electrochemistry Communications* **2007,** *9* (5), 1228-1232.

36. Scott, I. D.; Jung, Y. S.; Cavanagh, A. S.; An, Y.; Dillon, A. C.; George, S. M.; Lee, S.-H., Ultrathin Coatings on Nano-LiCoO2 for Li-Ion Vehicular Applications. *Nano Letters* **2011,** *11* (2), 414-418.

37. Tukamoto, H.; West, A. R., Electronic conductivity of LiCoO2 and its enhancement by magnesium doping. *Journal of the Electrochemical Society* **1997,** *144* (9), 3164-3168.

38. (a) Lee, K. T.; Cho, J., Roles of nanosize in lithium reactive nanomaterials for lithium ion batteries. *Nano today* **2011,** *6* (1), 28-41; (b) Lee, S.; Jeong, S.; Cho, J., Spinel LiCo0. 7Mn1. 3O4 Nanowire Clusters as Electrode Materials. *ChemSusChem* **2010,** *3* (11), 1260-1263.

39. Wang, Y.; Li, H.; He, P.; Hosono, E.; Zhou, H., Nano active materials for lithium-ion batteries. *Nanoscale* **2010,** *2* (8), 1294-1305.

40. Plichta, E.; Salomon, M.; Slane, S.; Uchiyama, M.; Chua, D.; Ebner, W.; Lin, H., A rechargeable Li/LixCoO2 cell. *Journal of power sources* **1987,** *21* (1), 25-31.

41. (a) Kikkawa, S.; Miyazaki, S.; Koizumi, M., Electrochemical aspects of the deintercalation of layered AMO2 compounds. *Journal of Power Sources* **1985,** *14* (1-3), 231-234; (b) Molenda, J., Correlation between electronic and electrochemical properties of A x MO 2-type electrode materials. Electronic criterion. *Solid State Ionics* **1986,** *21* (4), 263-272.

42. Jaafar, M.; Razak, K. A.; Ariff, Z. M.; Zabidi, H.; Aziz, N. A. A.; Abdullah, T. K.; Mohamad, A. A., 5th International Conference on Recent Advances in Materials, Minerals and Environment (RAMM) & 2nd International Postgraduate Conference on Materials, Mineral and Polymer (MAMIP)Synthesis of LiCoO2 Prepared by Sol–gel Method. *Procedia Chemistry* **2016,** *19*, 861-864.

43. Choi, S. H.; Kim, J.; Yoon, Y. S., Self-discharge analysis of LiCoO2 for lithium batteries. *Journal of Power Sources* **2004,** *138* (1–2), 283-287.

44. (a) Choi, Y.-M.; Pyun, S.-I., Determination of electrochemical active area of porous Li1−δCoO2 electrode using the GITT technique. *Solid State Ionics* **1998,** *109* (1–2), 159-163; (b) Li, Z.; Du, F.; Bie, X.; Zhang, D.; Cai, Y.; Cui, X.; Wang, C.; Chen, G.; Wei, Y., Electrochemical kinetics of the Li [Li0. 23Co0. 3Mn0. 47] O2 cathode material studied by GITT and EIS. *The Journal of Physical Chemistry C* **2010,** *114* (51), 22751-22757.